EEG and fMRI connectomes are reliably related: a simultaneous EEG-fMRI study from 1.5T to 7T

Jonathan Wirsich[1], João Jorge[2,3], Giannina R Iannotti[1], Elhum A Shamshiri[1], Frédéric Grouiller[4], Rodolfo Abreu[5,6], François Lazeyras[7], Anne-Lise Giraud[8], Rolf Gruetter[2,7,9], Sepideh Sadaghiani[10,11], Serge Vulliémoz[1]

[1]EEG and Epilepsy Unit, University Hospitals and Faculty of Medicine of Geneva, Geneva, Switzerland

[2]Laboratory for Functional and Metabolic Imaging, École Polytechnique Fédérale de Lausanne, Lausanne, Switzerland

[3]Systems Division, Swiss Center for Electronics and Microtechnology (CSEM), Neuchâtel, Switzerland

[4]Swiss Center for Affective Sciences, University of Geneva, Geneva, Switzerland

[5]ISR-Lisboa/LARSyS and Department of Bioengineering, Instituto Superior Técnico – Universidade de Lisboa, Lisbon, Portugal

[6]Coimbra Institute for Biomedical Imaging and Translational Research (CIBIT), Institute for Nuclear Sciences Applied to Health (ICNAS), University of Coimbra, Coimbra, Portugal

[7]Department of Radiology and Medical Informatics, University of Geneva, Geneva, Switzerland

[8]Department of Neuroscience, University of Geneva, Geneva, Switzerland

[9]Department of Radiology, University of Lausanne, Lausanne, Switzerland

[10]Beckman Institute, University of Illinois at Urbana-Champaign, Urbana, IL, USA

[11]Psychology Department, University of Illinois at Urbana-Champaign, Urbana, IL, USA

Abstract

Both electroencephalography (EEG) and functional Magnetic Resonance Imaging (fMRI) are non-invasive methods that show complementary aspects of human brain activity. Despite their differences in probing brain activity, both electrophysiology and BOLD signal can map the underlying functional connectivity structure at the whole brain scale at different timescales. Previous work demonstrated a moderate but significant correlation between resting-state functional connectivity of both modalities, however there is a wide range of technical setups to measure simultaneous EEG-fMRI and the reliability of those measures between different setups remains unknown. This is true notably with respect to different magnetic field strengths (low and high field) and different spatial sampling of EEG (medium to high-density electrode coverage).

Here, we investigated the reliability of the bimodal EEG-fMRI functional connectome in the most comprehensive resting-state simultaneous EEG-fMRI dataset compiled to date including a total of 72 subjects from four different imaging centers. Data was acquired from 1.5T, 3T and 7T scanners with simultaneously recorded EEG using 64 or 256 electrodes. We demonstrate that the whole-brain monomodal connectivity reliably correlates across different datasets and that the crossmodal correlation between EEG and fMRI connectivity of $r \approx 0.3$ can be reliably extracted in low and high-field scanners. The crossmodal correlation was strongest in the EEG-β frequency band but exists across all frequency bands. Both homotopic and withing intrinsic connectivity network (ICN) connections contributed the most to the crossmodal relationship.

This study confirms, using a considerably diverse range of recording setups, that simultaneous EEG-fMRI offers a consistent estimate of multimodal functional connectomes in healthy subjects being organized into reliable ICNs across different timescales. This opens new avenues for estimating the dynamics of brain function and provides a better understanding of interactions between EEG and fMRI measures. Alterations of this coupling could be explored as a potential clinical marker of pathological brain function.

Abbreviations

Amplitude envelope correlation	AEC
Electrocardiogram	ECG
Functional connectivity	FC
Independent component analysis	ICA
Intrinsic connectivity network	ICN
Imaginary part of the coherency	iCoh
Magneto/Electroencephalography	M/EEG
Structural connectivity	SC

Introduction

The brain is a complex system of interacting neurons continuously communicating with each other. This intrinsic brain functional connectivity (FC) has been shown to be organized in macro-scale patterns of interconnected regions, the so-called intrinsic connectivity networks (ICNs) (Biswal et al., 1995; Fox et al., 2005; Greicius et al., 2003). Though originally described for fMRI (FC_{fMRI}) data, those ICNs have also been found using Magnetoencephalography (MEG, FC_{MEG}) (Brookes et al., 2011) and Electroencephalography (EEG, FC_{EEG}) (Abreu et al., 2020; de Pasquale et al., 2010; de Pasquale et al., 2012; Finger et al., 2016; Wirsich et al., 2017). Expanding this initially network-specific view, cross-modal studies showed that FC in both electrophysiological (M/EEG) and BOLD signals are related when using static measures (averaged over periods >5 minutes) across the whole brain scale of resting-state recordings (Deligianni et al., 2014; Hipp and Siegel, 2015; Wirsich et al., 2017). Understanding the functional links between EEG- and fMRI-derived FC measures is a key question in current neuroimaging research, as it could help clarifying the neuronal substrates of both modalities, and of resting-state activity itself (Sadaghiani and Wirsich, 2020).

The relation between FC_{fMRI} and $FC_{M/EEG}$, has also been shown to be mediated by the underlying white matter structural connectivity derived from diffusion MRI (SC_{dMRI}) (Chu et al., 2015; Deligianni et al., 2019, 2016; Honey et al., 2009; Meier et al., 2016; Wirsich et al., 2017). Beyond the static relationship of EEG and fMRI to structure, we also observed crossmodal linked dynamics (1 minute sliding window) (Wirsich et al., 2020b). While most work focused on crossmodal agreement of FC, we have equally shown that the crossmodal connectivity can be split up into a common and complimentary connectivity profile across different timescales (Wirsich et al., 2020a). A crucial open question is whether crossmodal dissimilarities arise mainly from differences in data quality and acquisition setup, or represent differences arising from measuring complementary multimodal aspects of brain functional connectivity (Sadaghiani and Wirsich, 2020). In order to address this issue, data from independent research sites are needed. This would enable us to characterize the baseline relationship between connectivity derived from both modalities.

From a monomodal point of view, the reliability of FC_{fMRI} measures is well characterized (Noble et al., 2019) with a low intra class correlation (ICC=0.29) for individual connections and consistent ICN estimations across sites (Badhwar et al., 2020). While some of the variance stems from different scanner systems (Han et al., 2006) or inter-individual differences (Amico and Goñi, 2018; Finn et al., 2015), the chosen post-processing of data also introduces variability of the results (Botvinik-Nezer et al., 2020; Carp, 2012). Due to this connectivity variability, it is important to estimate the reliability of this measure, as a baseline for subsequent measures of alterations in different normal and pathological conditions (De Vico Fallani et al., 2014).

The reliability of $FC_{M/EEG}$ measures has been analyzed from different angles. Different measures of FC (Colclough et al., 2016) and multimodal acquisitions of FC using MEG and EEG (Coquelet et al., 2020) both result in highly correlated estimations of $FC_{M/EEG}$ and Marquetand et al. (2019) observed good intersession reliability (ICC>0.67) for both modalities. From a frequency point of view, alpha has been shown to be the most reliable estimate across subjects (Colclough et al., 2016; Marquetand et al., 2019). While the majority of FC_{fMRI} work derives connectivity from correlating regional timecourses of the BOLD signal, no consensus has been reached yet for $FC_{M/EEG}$, especially whether to use phase or amplitude coupling (Colclough et al., 2016; Sadaghiani and Wirsich, 2020). Both phase coupling using the

imaginary part of the coherency (iCoh) (Nolte et al., 2004; Wirsich et al., 2017) and amplitude coupling using amplitude envelope correlation (AEC) (Brookes et al., 2011; de Pasquale et al., 2010; Deligianni et al., 2014; Hipp and Siegel, 2015) have been linked to FC_{fMRI}. It has been argued that phase coupling might be closer to the underlying SC_{dMRI} and amplitude coupling is proposed to be more related to FC_{fMRI} (Engel et al., 2013). Nevertheless, most of the literature suggests a rather similar connectivity pattern on the whole brain scale when averaging over resting-state recordings lasting several minutes (Colclough et al., 2016; Mostame and Sadaghiani, 2020; Sadaghiani and Wirsich, 2020). Siems and Siegel (2020) observed highly correlated, but not identical connectivity between both types of measures, and the neurobiological interpretation of those differences have yet to be explored. Ultimately the relevance of different connectivity measures for brain behavior and pathology is still an open question.

Electrophysiological measures suffer from an ill-posed problem, when reconstructing sparsely sampled sensor signals on the scalp into the three-dimensional brain space, resulting in source-activity leaking into different regions which can distort connectivity measures (Palva et al., 2018). The selection of an optimal brain parcellation can reduce the variability arising from regional crosstalk due to source leakage of the inverse solution (Farahibozorg et al., 2018). Given those limitations of electrophysiological measures, less work has been done to extract electrophysiological connectomes (Sadaghiani and Wirsich, 2020). However, no study has compared if the EEG or the fMRI connectome can be measured more reliably across subjects, especially in a simultaneous recording.

In the case of simultaneous EEG-fMRI, signal quality is diminished by 1) artifacts on fMRI data induced by the EEG electrodes interacting with the static magnetic field and the MR-pulses (Mullinger et al., 2008b) 2) gradient- and pulse-related EEG artifacts induced by the magnetic gradients on the EEG electrodes and cables (Abreu et al., 2018; Allen et al., 2000). At 7T, EEG-fMRI can be affected by stronger recording artifacts (Abreu et al., 2016; Jorge et al., 2015b; Mullinger et al., 2008a; Neuner et al., 2013). Overcoming those limitations would encourage analysis of the dynamic electrophysiological correlates of BOLD signal at much higher temporal and spatial resolutions (Meyer et al., 2019; Scheeringa and Fries, 2017). Though it is well documented that the data quality of EEG and fMRI depends on scanner field strength (Debener et al., 2008; Mullinger et al., 2008b), no data exists assessing the impact on the data reliability at the level of functional connectivity. The possibility to compensate for the larger artifacts at higher field (Jorge et al., 2015a) might be sufficient to achieve reliable EEG-fMRI connectivity measures.

To close the gap of unknown reliability of EEG-fMRI connectomes across experimental setups and to evaluate the suitability of a 7T EEG-fMRI setup for multimodal connectomics in this study we aim to:

1) compare the monomodal reliability of FC_{fMRI} to FC_{EEG} derived from simultaneous EEG-fMRI across different imaging centers
2) characterize the reliability of crossmodal FC_{fMRI}-FC_{EEG} across heterogeneous setups and notably for the first time at 7T
3) characterize the spatial contributions of individual connections to this crossmodal relationship

We combined simultaneous EEG-fMRI resting state acquisitions from 4 different centers totaling 72 subjects, and comprising recordings using a 1.5T, 3T and 7T MR scanner in combination with a 64 or 256 EEG electrode system.

Methods

Subjects and acquisition setup

We analyzed a total of 72 subjects divided up into 4 datasets: 16 subjects using a 64-channel EEG setup in a 1.5T MR-scanner (64Ch-1.5T), 26 subjects using a 64 channel EEG setup in a 3T MR-scanner (64Ch-3T), 21 subjects using a 256 channel EEG setup in a 3T MR-scanner (256Ch-3T) and 9 subjects using a 64 channel EEG setup in a 7T MR-scanner (64Ch-7T). Main differences between study paradigm, hardware and software setup are summarized in SI Table 1.

Data set 1 (64Ch-1.5T)

16 subjects (6 females, mean age: 32.41, range 22-53) with no history of neurological or psychiatric illness were recorded. Ethical approval was given by local Research Ethics Committee (UCL Research ethics committee, project ID: 4290/001) and informed consent was obtained from all subjects (Deligianni et al., 2016, 2014). In each subject one run of 10 min 48 seconds resting-state simultaneous EEG-fMRI was acquired. Subjects were asked not to move, to remain awake and fixate on a white cross presented on a black background. MRI was acquired using a 1.5 Tesla MR-scanner (Siemens Avanto). The fMRI scan comprised of the following parameters: GRE-EPI sequence, TR=2160, TE=30ms, 30 slices, 210x210mm Field of View, voxel size 3.3x3.3x4.0mm^3 (1mm gap), flip angle 75°, total of 300 volumes. The subjects' head was immobilized using a vacuum cushion during scanning. Additionally, an anatomical T1-weighted image was acquired (176 sagittal slices, 1.0x1.0x1.0 mm, TA=11min). EEG was acquired using two 32-channel MR-compatible amplifiers (BrainAmp MR, sampling rate 1kHz), 63 electrodes (BrainCap MR, Gilching, Germany), referenced to FCz, 1 ECG electrode. The scanner clock was time-locked with the amplifier clock (Mandelkow et al., 2006). The MR-compatible amplifier was positioned behind outside the bore behind the head of the subject.

Data set 2 (64Ch-3T)

26 healthy subjects (8 females, mean age 24.39, age range 18-31) with no history of neurological or psychiatric illness were recorded. Ethical approval was given by local Research Ethics Committee (CPP Ile de France III) and informed consent was obtained from all subjects (Sadaghiani et al., 2010). In each subject, 3 runs of 10 minutes (total 30 mins) resting-state simultaneous EEG-fMRI were acquired. Subjects were asked not to move and to remain awake and keep their eyes closed during the resting-state scan. For three subjects, one out of the three rest sessions was excluded due to insufficient EEG quality. The resting-state sessions were part of a study with two additional naturalistic film stimuli of 10 minutes not analyzed in the current study, and acquired after resting runs 1 and 2 of the resting state as described in Morillon et al. (Morillon et al., 2010). MRI was acquired using a 3 Tesla MR-scanner (Siemens Tim-Trio). The fMRI scan comprised of the following parameters: GRE-EPI sequence, TR=2000ms, TE=50ms, 40 slices, 192x192mm Field of View, voxel size 3x3x3mm^3, flip angle 78°, total of 150 volumes (total all sessions 450 volumes). An anatomical T1-weighted image was acquired (176 sagittal slices, 1.0x1.0x1.0 mm, TA=7min). EEG was acquired using two 32-channel MR-compatible amplifiers (BrainAmp MR, sampling rate 5kHz), 62 electrodes (Easycap, Herrsching, Germany), referenced to FCz, 1 ECG electrode, and 1 EOG electrode. The scanner clock was time-locked with the amplifier clock (Mandelkow et al., 2006). The MR-compatible amplifier was positioned behind outside the bore behind the head of the subject.

Data set 3 (256Ch-3T)

21 healthy subjects (7 females, 32.13, age range 24-47) with no history of neurological or psychiatric illness were recorded. Ethical approval was given by local Research Ethics Committee (Ethics committee of Geneva) and informed consent was obtained from all subjects. A subgroup of this cohort has been already analyzed by (Iannotti et al., 2015). In each subject one run of 4min 58s resting-state simultaneous EEG-fMRI were acquired. Five subjects had a longer recording of 19min 52s and one subject had a recording of 9min 56s, in all those cases the total run was analyzed. Subjects were asked not to move and to remain awake and keep their eyes closed during the resting-sate scan. MRI was acquired using a 3 Tesla MR-scanner (Siemens Magnetom Trio). The fMRI scan comprised the following parameters: GRE-EPI sequence, TR=1990ms, TE=30ms, 32 slices, 192x192mm Field of View, voxel size 3x3x3.75mm^3, flip angle 90°, total of 150 volumes. Additionally, an anatomical T1-weighted image was acquired (176 sagittal slices, 1.0x1.0x1.0 mm, TA=7min). EEG was acquired using a 258-channel MR-compatible amplifier (Electrical Geodesic Inc., Eugene, OR, USA, sampling rate 1kHz), 256 electrodes (Geodesic Sensor Net 256), referenced to Cz, 2 ECG electrodes. The scanner clock was time-locked with the amplifier clock (Mandelkow et al., 2006). An elastic bandage was pulled over the subjects' head and EEG cap to assure the contact of electrodes on the scalp. The MR-compatible amplifier was positioned to the left of the subject and EEG and ECG cables were passed through the front end of the bore.

Data set 4 (64Ch-7T)

9 healthy subjects (4 females, mean age 23.56, age range 22-26) with no history of neurological or psychiatric illness were recorded. Ethical approval was given by the local Research Ethics Committee (CER-VD) and informed consent was obtained from all subjects (Jorge et al., 2019). In each subject 1 run of 8 minutes resting-state simultaneous EEG-fMRI was acquired. Subjects were asked not to move in the MR scanner and to keep their eyes open during the resting-state scan, fixating on a small red cross presented on a grey background, to minimize head and eye movements. Padding was also used to further restrict motion. MRI was acquired using a 7 Tesla head MR-scanner (Siemens Magnetom). The fMRI scan was performed using a simultaneous multi-slice (SMS) GRE-EPI sequence (3× SMS and 2× in-plane GRAPPA accelerations), with TR=1000ms, TE=25ms, 69 slices, 220×220mm Field of View, voxel size 2.2x2.2x2.2 mm, flip angle 54°, and a total of 480 volumes. A short EPI acquisition (5 volumes) with reversed phase encoding direction was also performed, for image distortion correction. Additionally, an anatomical T1-weighted image was acquired (160 sagittal slices, 1.0x1.0x1.0mm, TA = 10min). EEG was acquired using two 32-channel MR-compatible amplifiers (BrainAmp MR, sampling rate 5kHz), and a 63-electrode (EasyCap, Herrsching, Germany), referenced to FCz, 1 ECG electrode, connected via 12-cm bundled cables to reduce artifact contributions (Jorge et al., 2015b). Four of the 64 electrodes (T7, T8, F5 and F6) were customized to serve as motion artifact sensors (Jorge et al., 2015a). A total of 59 electrodes therefore remained dedicated to EEG recording. The scanner clock was time-synchronized with the amplifier clock (Mandelkow et al., 2006)). The MR-compatible amplifier was positioned inside the bore behind the head of the subject.

Analysis

As data acquisition already has a considerable number of varying parameters that might affect the final FC estimation, we stress here that also for the analysis we did not strictly control every processing step. The rationale of this was that independent of setup and postprocessing, the different datasets should generalize across a family of analysis (Botvinik-Nezer et al., 2020) and result in reliable monomodal and crossmodal measures.

Brain parcellation

We used the Freesurfer toolbox to process the T1-weighted images (recon-all, v6.0.0 http://surfer.nmr.mgh.harvard.edu/) in order to perform non-uniformity and intensity correction, skull stripping and grey/white matter segmentation. The cortex was parcellated into 148 regions according to the Destrieux atlas (Destrieux et al., 2010; Fischl et al., 2004) and into 68 regions according to the Desikan(-Killiany) atlas (Desikan et al., 2006). According to the results of Farahibozorg et al. (2018), showing that the optimal size of parcellation to capture independent EEG signals contains around 70 regions we decided to use the Desikan atlas as reference.

Specific strategy for 64Ch-7T: Due to local signal drops in the T1-weighted images near the EEG lead convergence points (Jorge et al., 2015b) we were not able to run the Freesurfer individual segmentation (recon-all) for all subjects. In order to not lose any of the subjects and to keep consistency within the data set we coregistered all fMRI images to the MNI template. We used Freesurfer to extract the surfaces of the MNI template. In order to account for subject specific variances, we dilated the atlas images by 3 voxels (using https://github.com/mattcieslak/easy_lausanne). The transformation of the segmented MNI template to fMRI was calculated by coregistering the fMRI images to the T1 image using FSL-FLIRT (6.0.2) (Jenkinson et al., 2002) with boundary-based registration using white matter masks obtained by segmentation with ANTS (version 2.2.0) (Avants et al., 2011). The T1 was coregistered to the MNI template using FSL-FNIRT (6.0.2) (Jenkinson and Smith, 2001).

fMRI processing

Slice timing correction was applied to the fMRI timeseries (for the Ch64-3T and Ch256-3T datasets only). This was followed by spatial realignment using the SPM12 toolbox (Ch64-1.5T/Ch64-3T: revision 6906; Ch256-3T/Ch64-7T revision 7475; http://www.fil.ion.ucl.ac.uk/spm/software/spm12). A coregisteration (FSL-FLIRT 6.0.2) of the T1 images of each subject and the Desikan/Destrieux atlas to the fMRI images was carried out. We extracted signals of no interest such as the average signals of cerebrospinal fluid (CSF) and white matter from manually defined regions of interest (ROI, 5mm sphere, Marsbar Toolbox 0.44, http://marsbar.sourceforge.net) and regressed out of the BOLD timeseries along with 6 rotation, translation motion parameters and global gray matter signal (Wirsich et al., 2017). Then we bandpass-filtered the timeseries at 0.009-0.08 Hz (Power et al., 2014) and scrubbed it using frame wise displacement (threshold 0.5) as defined by Power et al. (Power et al., 2012).

Specific strategy for 64Ch-7T: Data was also B0-unwarped before spatial alignment, using FSL-TOPUP (6.0.2) (Andersson et al., 2003), based on the reverse-encoding reference acquisition, to mitigate the more accentuated image distortions present at 7T (Jorge et al., 2018). Given the short TR of 1s no slice timing correction was carried out.

Specific strategy for 64Ch-1.5T: In order to stick to the original processing of (Deligianni et al., 2014) no slice timing correction was carried out.

fMRI connectivity measures

Average timeseries of each region was then used to calculate FC_{fMRI} by taking the pairwise Pearson correlation of each regions' cleaned timecourse (see schema Fig 1).

EEG processing

EEG data was preprocessed individually for the different setups:

64Ch-1.5T: EEG was corrected for the scanner gradient artifact using template subtraction, adaptive noise cancellation and downsampling to 250Hz (Allen et al., 2000) followed by pulse-related artifact template subtraction (Allen et al., 1998). Then ICA-based denoising (for removal of gradient and pulse artifact residuals, eye-blinks, muscle artifacts) using the Brain Vision Analyzer 2 software (Brain Products, Gilching, Germany) was carried out.

64Ch-3T: EEG was corrected for the scanner gradient artifact using template subtraction, adaptive noise cancellation followed by lowpass filtering at 75Hz, downsampling to 250Hz (Allen et al., 2000). Then pulse-related artifact template subtraction (Allen et al., 1998) using EEGlab v.7 (http://sccn.ucsd.edu/eeglab) and the FMRIB plug-in (https://fsl.fmrib.ox.ac.uk/eeglab/fmribplugin/) was carried out.

256Ch-3T: EEG was corrected for the scanner gradient artifact using template subtraction with optimal basis set and adaptive noise cancellation (Allen et al., 2000; Niazy et al., 2005), followed by pulse-related artifact template subtraction (Allen et al., 1998) using in-house code Matlab code for ballistocardiogram peak detection as described in (Iannotti et al., 2015). Electrodes placed on the cheeks and in the face were excluded form data analysis resulting in final 204 used electrodes. This was followed by manual ICA-based denoising (for removal of gradient and pulse artifact residuals, eye-blinks, muscle artifacts, infoMax, runICA-function EEGLab revision 1.29 (Bell and Sejnowski, 1995; Delorme and Makeig, 2004))

64Ch-7T: EEG data pre-processing included the following steps: gradient artifact correction using template substraction (as described in (Jorge et al., 2015a)), bad channel interpolation (1–4 channels per subject), temporal band-pass filtering (1–70 Hz), pulse-related artifact correction (using a k-means clustering-based approach validated in (Jorge et al., 2019) in line with (Gonçalves et al., 2007)), downsampling to 500 Hz, motion artifact correction (offline multi-channel recursive least-squares regression, using the motion sensor signals, as described in (Jorge et al., 2015a)), and manual ICA-based denoising (for removal of e.g. gradient and pulse artifact residuals, eye-blinks, muscle artifacts, inhouse ICA extended Infomax algorithm).

All datasets: Cleaned EEG data was analyzed with Brainstorm software (Tadel et al., 2011), which is documented and freely available under the GNU general public license (http://neuroimage.usc.edu/brainstorm, 64Ch-1.5T and 64Ch-3T data set: version 10th August 2017 as according to (Wirsich et al., 2020b), 256Ch-3T and 64Ch-3T data set: version 15th January 2019). Data was bandpass-filtered at 0.3-70 Hz (64Ch-1.5T at 0.5-70Hz, 64Ch-7T at 1-70Hz). Data was segmented according to one TR or as a multiple TRs of the fMRI acquisition (64Ch-1.5: 2160ms, 64Ch-3T: 2000ms, 256Ch-3T: 1990ms, 64Ch-7T: sliding window of 4000ms with 1000ms (1TR) steps).

EEG epochs containing motion were semi-automatically detected if the signal in any channel exceeded the mean channel timecourse by 4 standard deviations. Then the whole timecourse was also visually inspected to exclude all motion segments from further analysis. Electrode positions and T1 were coregistered by manually aligning the electrode positions onto the electrode artifacts visible in the T1 image. A forward model of the skull was calculated based on the individual T1 image of each subject using the OpenMEEG BEM model (Gramfort et al., 2010; Kybic et al., 2005). The EEG signal was projected into source space using the Tikhonov-regularized minimum norm (Baillet et al., 2001) with the Tikhonov parameter set to 10% (Ch64-1.5T/Ch64-3T brainstorm 2016 implementation and Ch256-3T/Ch64-7T brainstorm 2018 implementation, assumed SNR ratio 3.0, using current density maps, constrained sources normal to cortex/signs were flipped into one direction, depth weighting 0.5/max

amount 10). Finally, source activity was averaged in each cortical region of the Desikan and the Destrieux atlas.

EEG connectivity measures

For each epoch the imaginary part of the coherency (iCoh) of the source activity was calculated between each region pair (cortical regions only: Desikan atlas - 68 regions or Destrieux atlas - 148 regions) using bins of 2Hz frequency resolution (Nolte et al., 2004; Wirsich et al., 2020a, 2017). The 2Hz bins were averaged for 5 canonical frequency bands: delta (δ 0.5-4Hz, 64Ch-7T: at 1-4Hz), theta (θ 4-8Hz), alpha (α 8-12Hz), beta (β 12-30Hz), gamma (γ 30-60Hz). The segments were then averaged for each subject to one FC_{EEG} matrix.

We calculated the amplitude envelope correlation (AEC) of the signal by taking the Hilbert envelope of the unsegmented data of each subject filtered into the canonical frequency bands both for the Destrieux and Desikan atlas. We calculated the correlation of the filtered data both without (Deligianni et al., 2014; Glomb et al., 2020) and with (Brookes et al., 2012; Hipp et al., 2012) a subsequent pairwise orthogonalization approach to attenuate crosstalk between signals ($AEC_{non\text{-}orthogonalized}$/$AEC_{orthogonalized}$, Brainstorm implementation, version 27-01-2019).

Reliability

We assessed the modality-specific reliability by calculating the monomodal inter-dataset correlation between averaged FC_{fMRI} (of each dataset across all runs and subjects). The same analysis was performed for FC_{EEG} (in each frequency band). Intra-dataset monomodal reliability was assessed by splitting up each dataset into two halves and calculating the correlation of the average connectome between both halves.

We then assessed the crossmodal correlation between FC_{fMRI} and FC_{EEG} for each EEG frequency band across different configurations (brain atlas, EEG connectivity measure). Effects on the crossmodal FC_{EEG}-FC_{fMRI} correlation due to EEG frequency bands (δ, θ, α, β, γ), atlas choice (Desikan vs. Destrieux), EEG connectivity measure (iCoh, $AEC_{non\text{-}orthogonalized}$, $AEC_{orthogonalized}$) were assessed on the average connectome of each dataset (permutation test with 5000 iterations, testing the effects against average connectomes with switched labels at the individual level, in order to be able to compare the 2278 connections of the Desikan atlas to the 11026 connections of the Destrieux atlas we randomly drew 2278 out of the 11026 Destrieux connections for each iteration).

To assess the effect of small sample sizes and short recording length we cut all datasets to a recording length of the first 5 minutes (according to the recording length in dataset 256Ch-3T). Then we took only the first nine subjects of each dataset to calculate the connectome average of EEG and fMRI (according to the number of subjects in dataset 64Ch-7T). Significance was tested by switching labels between 5 minute and full-length data and by comparing the crossmodal correlation of all subjects against 9 randomly sampled subjects.

Spatial characterization

Focusing on the multimodal connectomes in the Desikan atlas averaged over all datasets, we assessed the relative contribution of each connection to the correlation between FC_{EEG} and FC_{fMRI} according to Colclough et al. (2016). The relative contribution c of each connection I is given by: $c_i = \frac{z_i^x z_i^y}{\sum_i z_i^x z_i^y} = \frac{z_i^x z_i^y}{r}$ with $z_i^x = \frac{x_i - \langle x \rangle}{\sqrt{\sum_i (x_i - \langle x \rangle)^2}}$ given the Pearson correlation coefficient of two vectors x and y:

. The resulting spatial contribution matrix was then correlated across the different datasets to assess the reliability of this spatial contribution to the crossmodal relationship. To classify the results we mapped the 68 regions of the Desikan atlas to 7 canonical ICNs (VIS: Visual, SM: Somatomotor, DA: Dorsal Attention, VA: Ventral Attention, L: Limbic, FP: Fronto-Parietal, DMN: Default Mode Network) (Amico et al., 2017; Yeo et al., 2011) and we subdivided the connections into homotopic, intrahemispheric and interhemispheric connections. We tested if the spatial contribution to the crossmodal correlation was more prominent for each ICN, for homotopic connections and for interhemispheric connections (one-sided ttest). Finally, we tested if the magnitude of the crossmodal correlation was increased for each ICN, for homotopic connections and for intrahemispheric connections (one-sided ttest).

Crossmodal correlation from single subject to the average connectome

Besides taking the average multimodal connectome of each dataset we also calculated the correlation between EEG and fMRI connectomes in each subject. Using a two-way ANOVA we tested if the crossmodal correlation differs in terms of the dataset and EEG frequency band. Additionally to limiting the subject average to 9 subjects, in order to better understand the relationship between single subject and dataset-averaged estimates we aimed to define the number of subjects needed for a reliable averaged connectome. To do so now and randomly selected 1,2,…,n subjects (5000 iterations each step) and averaged the EEG and fMRI connectomes of the selected subjects. Then we calculated the correlation between FC_{EEG} and FC_{fMRI} for each of the subject steps. We repeated this approach for the combined dataset sampling a mean correlation between the mean EEG and fMRI connectome from n randomly drawn subjects. To determine how many subjects are needed for a stable average connectome we took the average crossmodal correlation over all subjects of each frequency band as reference correlation. We then compared 1% of reference correlation to the change rate when adding one random subject (5000 iterations). The crossmodal correlation was considered stable when the change rate did not differ more than 1% of the total crossmodal reference correlation.

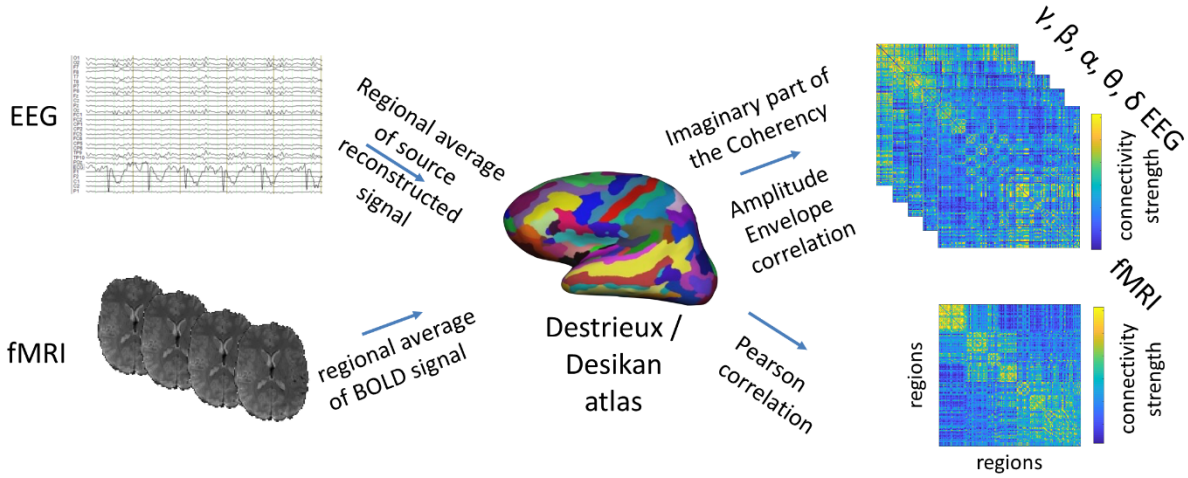

Fig 1: Construction of EEG and fMRI connectomes. EEG and fMRI data were parcellated into the 148 cortical regions of the Destrieux atlas (and 68 regions of the Desikan atlas) as follows: EEG was source reconstructed to a fine-grained grid, and the timecourses of the solution points were averaged per region and per subject. For fMRI, the BOLD signal timecourse was averaged over the voxels in each region for each subject. Pearson correlation of the average fMRI-BOLD timecourses and imaginary part of the coherency (iCoh) / envelope amplitudes correlation (AEC, orthogonalized and non-orthoginalized) of

averaged EEG source signals were used to build functional connectivity matrices / connectomes (FC_{EEG} and FC_{fMRI} for each subject (adapted from (Wirsich et al., 2020a))

Results

Unimodal and multimodal reliability between datasets

We measured unimodal reliability by taking correlations of connectivities of each modality. Between datasets, unimodal connectivity matrices were all correlated for both modalities (Table 1, Table 2). 7T fMRI data correlated less with the other datasets (Table 1), EEG correlations were lower than correlations between fMRI (Table 1, Table 2). In terms of inter-dataset connectome correlation, delta, theta and beta band connectomes were the most correlated across datasets (r>0.65, see Table 2). Unlike otherwise stated, the results of this section are all derived from the group-averaged connectomes of each dataset.

Table 1:Interdataset correlation of FC_{fMRI}. The off-diagonals (orange) show the inter-dataset correlation of dataset-average fMRI connectome (Desikan atlas) between the different datasets, the diagonals show the intra-dataset correlation of the dataset split-half averaged fMRI connectome

	64Ch-1.5T	**64Ch-3T**	**256Ch-3T**	**64Ch-7T**
64Ch-1.5T	0.81	0.81	0.78	0.69
64Ch-3T		0.95	0.90	0.69
256Ch-3T			0.88	0.64
64Ch-7T				0.78

Table 2: Interdataset correlation of FC_{EEG}. The off-diagonals (orange) show the inter-dataset correlation correlation of dataset-averaged EEG connectome (Desikan atlas, imaginary part of the coherency) between the different datasets, the diagonals show the intra-dataset correlation of the dataset split-half averaged EEG connectome

	64Ch-1.5T	**64Ch-3T**	**256Ch-3T**	**64Ch-7T**
Delta				
64Ch-1.5T	0.79	0.81	0.68	0.66
64Ch-3T		0.82	0.75	0.71
256Ch-3T			0.76	0.68
64Ch-7T				0.78
Theta				
64Ch-1.5T	0.76	0.83	0.68	0.66
64Ch-3T		0.88	0.77	0.71
256Ch-3T			0.79	0.72
64Ch-7T				0.80
Alpha				
64Ch-1.5T	0.70	0.63	0.76	0.71
64Ch-3T		0.85	0.57	0.51
256Ch-3T			0.75	0.73
64Ch-7T				0.77

Beta				
64Ch-1.5T	0.85	0.84	0.85	0.73
64Ch-3T		0.90	0.79	0.64
256Ch-3T			0.81	0.69
64Ch-7T				0.79
Gamma				
64Ch-1.5T	0.77	0.69	0.43	0.68
64Ch-3T		0.82	0.57	0.57
256Ch-3T			0.47	0.47
64Ch-7T				0.64

Crossmodal correlation of group-averaged EEG and fMRI connectomes

Correlations between EEG and fMRI were highest for the beta band, while gamma and delta band were the most variable across datasets. A grand average across all datasets (72 subjects) resulted in the highest correlation between EEG and fMRI for all bands (Fig 2a). While subject averaged FC_{fMRI}-$FC_{EEG-\beta}$ correlation was significantly higher than all the other bands ($p<0.0002$, permutation test, see SI Table 3), the subject averaged FC_{fMRI}-$FC_{EEG-\alpha}$ correlation was significantly increased only when compared to FC_{fMRI}-$FC_{EEG-\gamma}$ $p=0.0084$, 5000 permutations of frequency-band labels, see SI Table 3).

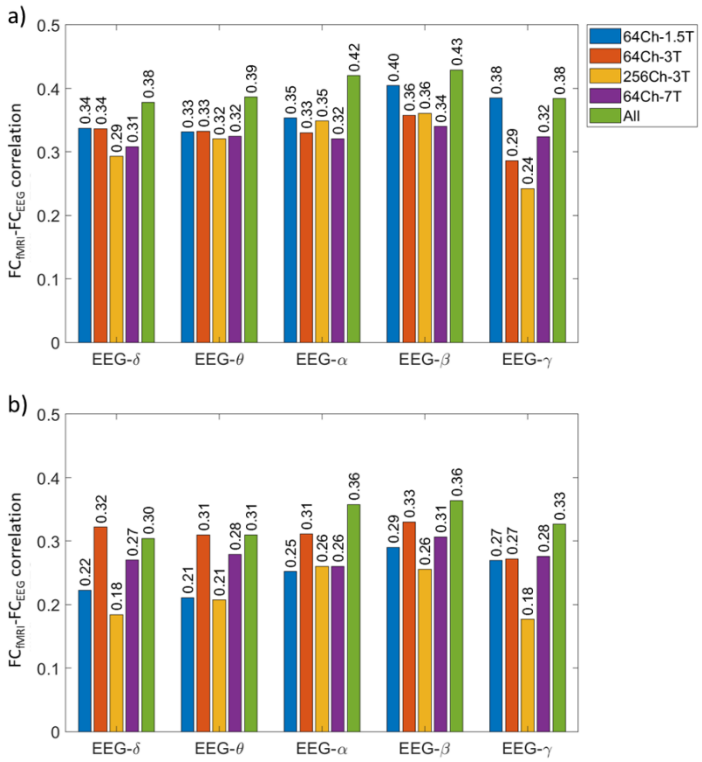

Fig 2: a) Crossmodal correlation dataset-averaged EEG and fMRI connectomes using the Desikan atlas (FC_{EEG} measure: imaginary part of the coherency); b) Crossmodal correlation dataset-averaged EEG and fMRI connectomes using the Destrieux atlas (FC_{EEG} measure: imaginary part of the coherency).

Crossmodal correlation of group averaged EEG and fMRI connectomes using an alternative atlas and alternative EEG connectivity measures

In this section we compared the above used atlas (Desikan) and EEG connectivity measures (iCoh) to alternatives. Taking an atlas with higher resolution resulted in a reduction of crossmodal FC_{fMRI}-FC_{EEG} correlation averaged over all datasets (Fig 2b, 5000 permutations, $p<0.0002$ for all frequency bands, see SI Table 4, a subset of the Destrieux connections were randomly chosen for each iteration to match the number of connections of the Desikan atlas: see methods). When using $AEC_{non\text{-}orthogonal}$ as FC_{EEG} connectivity measure crossmodal correlation increased as compared to taking iCoh (Fig 3b, for $FC_{EEG\text{-}\gamma}$ only, averaged over all datasets, permutation test 5000 iterations, SI Table 5), the orthogonalization approach ($AEC_{orthogonal}$) resulted in lower correlation compared to the iCoh (Fig 3b, all EEG frequency bands, 5000 permutations, $p<0.0002$, see SI Table 5). We did not find any significant correlation between FC_{fMRI} and $FC_{EEG\text{-}\gamma}$ in the 256Ch-3T dataset.

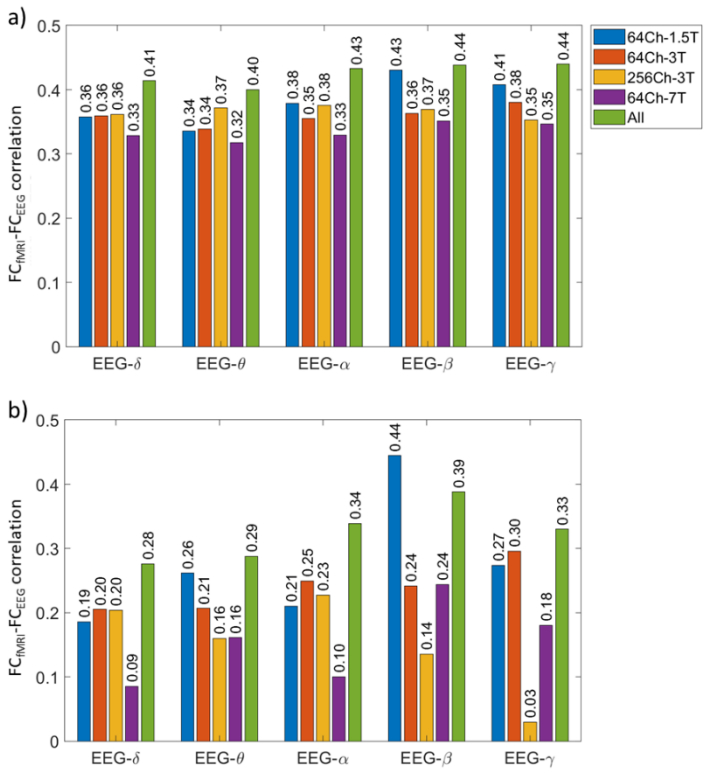

Fig 3: Crossmodal correlation dataset-averaged EEG and fMRI connectomes using Amplitude envelope correlation (AEC) to derive FC_{EEG} a) non-orthogonalized AEC and b) orthogonalized AEC (results for Desikan atlas)

Effect of number of subjects and length of resting-state recording on the crossmodal correlation

Next connectomes were cut down to the session length of the shortest dataset (5 min, Fig 4a) and subject averages were calculated using the same number of subjects (9 subjects, Fig 4b). The crossmodal correlation averaged over all datasets is not significantly different when the sessions are cut down to the first 5 minutes (permutation test 5000 iterations, all frequency bands, SI Table 6). When taking the average connectivity of only the first 9 subjects the crossmodal correlation between FC_{fMRI} and $FC_{EEG\text{-}\gamma}$ decreases significantly ($p=0.0006$, permutation 5000 iterations, SI Table 6)

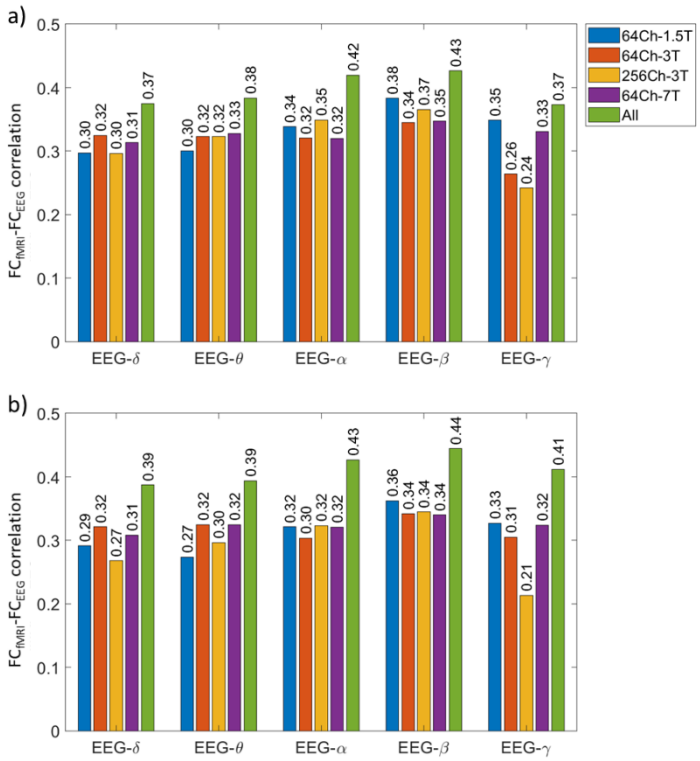

Fig 4: Crossmodal correlation between dataset-averaged EEG and fMRI connectomes limiting all datasets to: a) the first 5 minutes of each subject's session (according to the session length of the 256Ch-3T dataset) and b) the first 9 subjects of each dataset (according to the number of subjects of the 64Ch-7T dataset).

Spatial characterization of differences and ICN crossmodal correlation

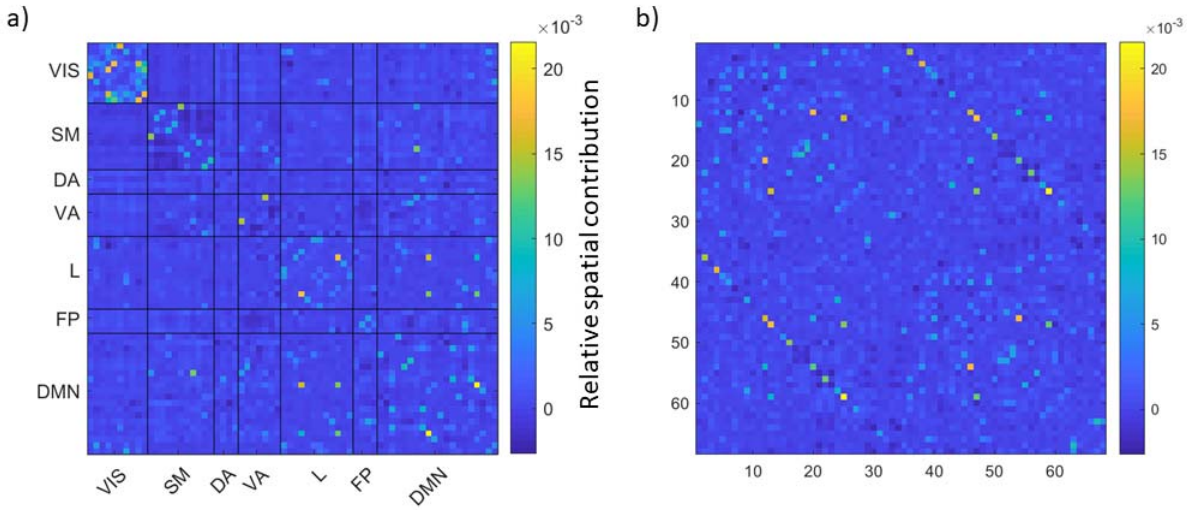

Fig 5: Relative spatial contribution (see methods) of each connection to the crossmodal correlation between $FC_{EEG\text{-}\theta}$ and FC_{fMRI} based on the average over all 72 subjects. (a) Spatial contribution is ordered according to the 7 canonical ICNs (Yeo et al. 2010). The Visual Network and the Limibic Network contributed the most to the crossmodal relationship. (b) Spatial contribution is ordered according to the two hemispheres. Off-diagonals highlight the homotopic connections that contributed the most to the

crossmodal correlation. Abbreviations: VIS: Visual, SM: somatomotor, DA: dorsal attention, VA: ventral attention, L: Limbic, FP: Fronto parietal, DMN: default mode network

We defined the connections that contribute most to the FC_{fMRI}-FC_{EEG} correlation using the connectomes averaged over all datasets (Colclough et al., 2016). Table 3 shows that this spatial contribution is reliably correlated between all datasets. The visual network contributes the most to the crossmodal correlation as well as the homotopic connections (Fig 5). Connections of the visual network contributed significantly more to the crossmodal FC_{fMRI}-FC_{EEG} correlation as compared to inter-ICN connections for all frequency bands (t-test spatial contribution Visual>interICN: FC_{fMRI}-$FC_{EEG-\delta}$/$FC_{EEG-\theta}$/$FC_{EEG-\alpha}$/$FC_{EEG-\beta}$/$FC_{EEG-\gamma}$; $p=3.2*10^{-47}/1.8*10^{-34}/p=5.1*10^{-69}/p=4.1*10^{-53}/1.5*10^{-81}$, Bonferroni correction threshold for 5 frequencies and 7 ICNs is defined at p=0.05/35=0.0014). Connections of the limbic network contributed significantly more to the FC_{fMRI}-FC_{EEG} correlation as compared to inter-ICN connections for all frequency bands except EEG-γ (t-test spatial contribution Limbic>inter-ICN: FC_{fMRI}-$FC_{EEG-\delta}$/$FC_{EEG-\theta}$/$FC_{EEG-\alpha}$/$FC_{EEG-\beta}$; $p=5.4*10^{-06}/4.3*10^{-06}/4.6*10^{-05}/3.2*10^{-05}$, Bonferroni correction threshold for 5 frequencies and 7 ICNs is defined at p=0.05/35=0.0014).

Homotopic connections contributed significantly more to the FC_{fMRI}-FC_{EEG} correlation as compared to the rest of the connectome for all bands (t-test spatial contribution homotopic>other connections: FC_{fMRI}-$FC_{EEG-\delta}$/$FC_{EEG-\theta}$/$FC_{EEG-\alpha}$/$FC_{EEG-\beta}$/$FC_{EEG-\gamma}$: $p=2.1*10^{-52}/8.710*10^{-50}/4.3*10^{-52}/p=1.2*10^{-55}/9.6*10^{-56}$, Bonferroni correction threshold for 5 frequencies is defined at p=0.05/5=0.01). Equally intrahemispheric connections contributed significantly more than interhemispheric connections (t-test spatial contribution intrahemispheric>interhemispheric: FC_{fMRI}-$FC_{EEG-\delta}$/$FC_{EEG-\theta}$/$FC_{EEG-\alpha}$/$FC_{EEG-\beta}$/$FC_{EEG-\gamma}$: $p=1.1*10^{-13}/1.3*10^{-14}/1.6*10^{-16}/9.3*10^{-23}/5.9*10^{-28}$, Bonferroni correction threshold for 5 frequencies is defined at p=0.05/5=0.01)

Table 3: Interdataset correlation of spatial regions specific contributions to the averaged FC_{fMRI}-FC_{EEG} crossmodal correlation

Spatial contribution	**64Ch-1.5T**	**64Ch-3T**	**256Ch-3T**	**64Ch-7T**
Delta				
64Ch-1.5T	x	0.76	0.62	0.64
64Ch-3T		x	0.76	0.64
256Ch-3T			x	0.61
Theta				
64Ch-1.5T	x	0.76	0.65	0.61
64Ch-3T		x	0.78	0.62
256Ch-3T			x	0.64
Alpha				
64Ch-1.5T	x	0.56	0.75	0.76
64Ch-3T		x	0.62	0.50
256Ch-3T			x	0.69
Beta				
64Ch-1.5T	x	0.81	0.80	0.74
64Ch-3T		x	0.84	0.65
256Ch-3T			x	0.66
Gamma				
64Ch-1.5T	x	0.79	0.66	0.70

64Ch-3T		x	0.71	0.66
256Ch-3T			x	0.61

To follow up we explored at the crossmodal correlation of FC_{fMRI}-FC_{EEG} while only selecting connections inside one ICN. When comparing the crossmodal correlation inside the different canonical ICNs to the crossmodal correlation of random in-between network connections of the same network size (randomly sampled, 5000 iterations), we observe a higher correlation in the Visual network ($r_{fMRI,EEG-\alpha}$ =0.61 ($r>r_{random}$: p=0.028), $r_{fMR,EEG-\gamma}$=0.63 ($r>r_{random}$: p=0.007), the Limbic network ($r_{fMRI,EEG-\delta}$=0.56, ($r>r_{random}$: p=0.03), $r_{fMRI,EEG-\beta}$=0.59 ($r>r_{random}$: p=0.022), $r_{fMRI,EEG-\gamma}$=0.60 ($r>r_{random}$: p=0.0034)) and the DMN ($r_{fMRI,EEG-\gamma}$=0.52 ($r>r_{random}$: p<0.0002), all significant at uncorrected threshold p<0.05, Bonferroni correction threshold is defined at p=0.05/35=0.0014).

Reliability of crossmodal correlation in individual connectomes

We generally observed the same distribution of FC_{EEG}-FC_{fMRI} correlation in individual as compared to the dataset average such as high crossmodal correlation for $FC_{EEG-\beta}$ and low crossmodal correlation for $FC_{EEG-\gamma}$ (Table 4). Lowest correlation was observed in the 256Ch-3T dataset.

A 2-way ANOVA of the individual subject crossmodal correlation revealed a significant main effect of datasets F(3, 71)=36.61, p=$1.6*10^{-20}$; and a significant main Effect of EEG Frequency bands F(4, 71)=6.85, p=$2.6*10^{-5}$. The interaction term dataset*band was not significant (F(12, 71)=1.32, p=0.21, significance threshold p<0.05). Tukey Posthoc t-tests on the main effect of the datasets established the following order of correlation magnitude: 64Ch-3T>64Ch-7T>64Ch-1.5T>256Ch-3T (64Ch-3T > 64Ch-1.5T (p<0.0001), 64Ch-3T>64Ch-7T (p=0.0031), 64Ch-3T>256Ch-3T (p<0.0001); 64Ch-7T>256Ch-3T (p=0.003)). Tukey Posthoc t-tests on the main effect of EEG frequency bands revealed that FC_{fMRI}-$FC_{EEG-\gamma}$ correlation was significantly smaller than FC_{fMRI}-$FC_{EEG-\beta}$ (p<0.0001) and FC_{fMRI}-$FC_{EEG-\theta}$ correlation (p=0.027).

Table 4: Average crossmodal correlation between EEG and fMRI connectomes of individuals across each dataset and frequency band (standard deviation in brackets)

	64Ch-1.5T	64Ch-3T	256Ch-3T	64Ch-7T	All datasets
FC_{fMRI}-$FC_{EEG-\delta}$	0.13 (0.05)	0.20 (0.05)	0.12 (0.04)	0.15 (0.04)	0.15 (0.06)
FC_{fMRI}-$FC_{EEG-\theta}$	0.12 (0.04)	0.19 (0.06)	0.13 (0.05)	0.16 (0.06)	0.15 (0.06)
FC_{fMRI}-$FC_{EEG-\alpha}$	0.12 (0.05)	0.18 (0.06)	0.13 (0.05)	0.16 (0.05)	0.15 (0.06)
FC_{fMRI}-$FC_{EEG-\beta}$	0.16 (0.04)	0.22 (0.06)	0.14 (0.04)	0.17 (0.04)	0.17 (0.06)
FC_{fMRI}-$FC_{EEG-\gamma}$	0.14 (0.05)	0.14 (0.06)	0.08 (0.05)	0.13 (0.04)	0.12 (0.06)

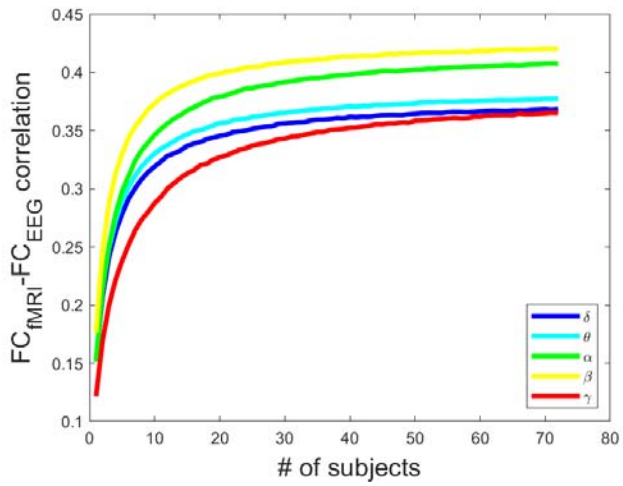

Fig 6: Subjects were randomly sampled from all datasets taking 1…n subjects (5000 iterations) then the crossmodal correlation between the EEG and fMRI connectome of each frequency band was calculated, the crossmodal correlation does not change after averaging around 7-12 subjects (see SI Table 2). For maximum correlation see also Fig 2 (all datasets).

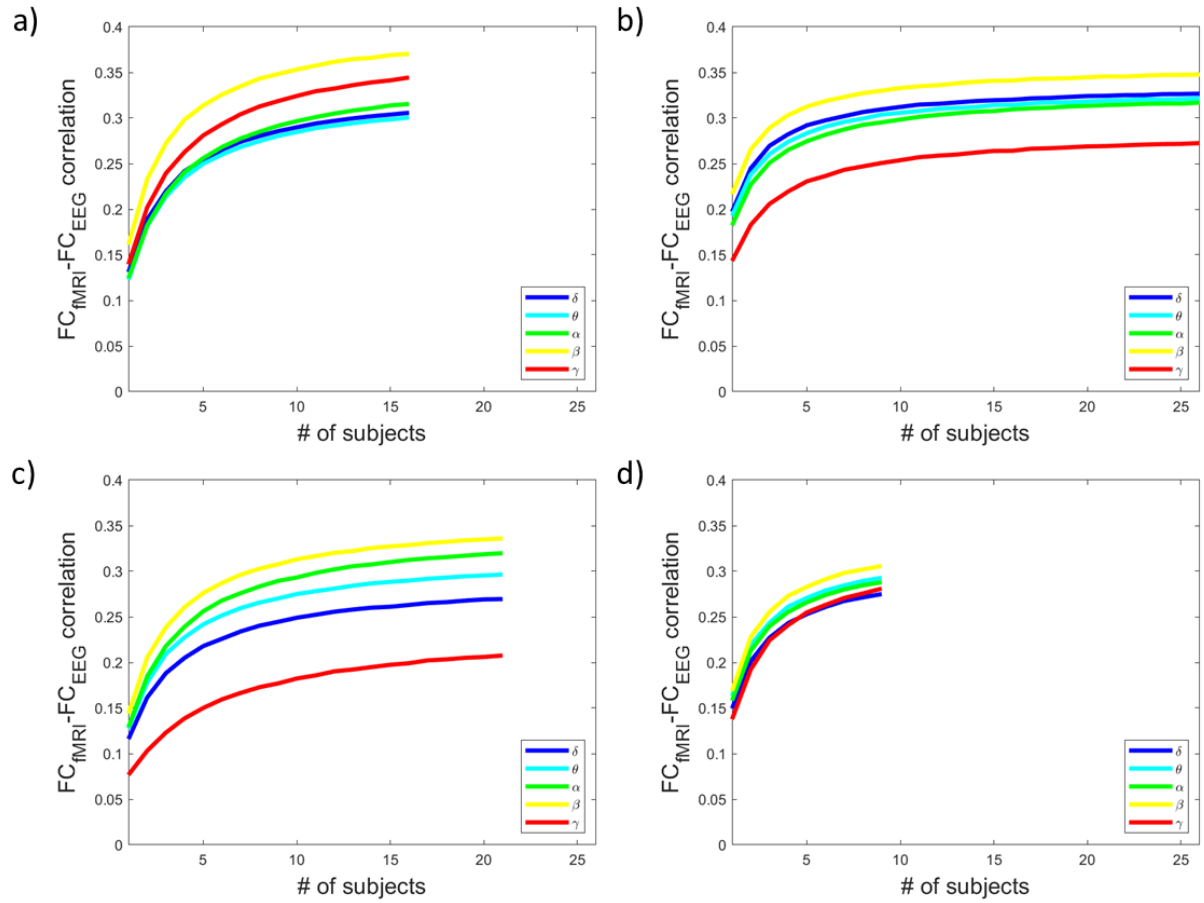

Fig 7: Subjects were randomly sampled for each dataset separately taking 1…n subjects (5000 iterations) then the crossmodal correlation between FC_{fMRI} and the FC_{EEG} of each frequency band was calculated, correlation does not change after averaging around 7-12 subjects (SI Table 2). a) 64Ch-1.5T b) 64Ch-3T c) 256Ch-3T d) 64Ch-7T. While the crossmodal correlation is

maximum for FC_{fMRI}-$FC_{EEG-\theta}$ FC_{fMRI}-$FC_{EEG-\gamma}$ is lowest for all datasets except the 64Ch-1.5 dataset (a). For the average crossmodal correlation across each dataset see also Fig 2.

$FC_{EEG-\beta}$ correlates the best with FC_{fMRI} for all datasets (Fig 6, Fig 7). On the contrary $FC_{EEG-\gamma}$-FC_{fMRI} was dependent on the data set showing the 2nd strongest correlation for the 64Ch-1.5T dataset and being by far the lowest correlation for the 64Ch-3T and 256Ch-3T dataset (Fig 7). Independent of the magnitude of the crossmodal correlation of each EEG frequency band, the crossmodal correlation was observed to be stable for each dataset when averaging 7-12 subjects (stable = adding 1 subject did not change the correlation more than 1% of the total crossmodal correlation when averaging connectomes over 72 subjects, SI Table 2). Combining all dataset to one average connectome maximized the crossmodal relationship for between FC_{fMRI} and $FC_{EEG-\delta}$, $FC_{EEG-\theta}$, $FC_{EEG-\alpha}$ and $FC_{EEG-\beta}$ but not for $FC_{EEG-\gamma}$. The 64Ch-1.5T dataset has an exceptionally high crossmodal correlation between $FC_{EEG-\gamma}$ and FC_{fMRI}. Consequently the correlation is not increased by taking the average of all 72 subjects (and effect clearly observed for all other bands Fig 2a: 64Ch-1.5T dataset: $r(FC_{EEG-\gamma}, FC_{fMRI})=0.38$ vs. all datasets: $r(FC_{EEG-\gamma}, FC_{fMRI})=0.39$).

Discussion

This study showed that the crossmodal correlation between EEG and fMRI connectivity can be simultaneously recorded with high reliability from a variety of experimental setups and designs, notably different MR magnetic fields and EEG electrode configurations (unimodal connectivity correlation for EEG and fMRI r~0.5-0.9 between all datasets and crossmodal connectivity correlation r~0.3-0.4 across all datasets). Of special note, we demonstrated for the first time that concurrent EEG and fMRI connectomes derived from 7T show the same unimodal and crossmodal correlations as compared to data from 1.5T and 3T. From an EEG-frequency point of view the crossmodal correlation was highest for FC_{fMRI}-$FC_{EEG-\beta}$, while from a spatial point of view the visual network and homotopic connections provided the most to the crossmodal correlation. When averaging subjects across all datasets, the correlation reaches a stable value from 7-12 subjects (see Fig 6, SI Table 2).

Frequency specific contributions

When combining all datasets $FC_{EEG-\alpha}$ and $FC_{EEG-\beta}$ correlated best with FC_{fMRI} ($r_{fMRI-EEG-\alpha}=0.41$ and $r_{fMRI-EEG-\beta}=0.43$, average over all datasets, see Fig 2a). The weaker crossmodal correlation between $FC_{EEG-\gamma}$/$FC_{EEG-\delta}$ and FC_{fMRI} is in line with previous findings (Tewarie et al., 2016; Wirsich et al., 2017). These results suggest that, besides band-specific SNR observed in our unimodal reliability (which would predict the strongest crossmodal coupling between FC_{fMRI} and $FC_{EEG-\alpha}$ instead of $FC_{-EEG-\beta}$ (Colclough et al., 2016; Marquetand et al., 2019)), frequency specific FC_{fMRI}-FC_{EEG} correlation can advance the functional understanding of large-scale connectivity. Specifically, the especially strong tie between $FC_{EEG-\alpha}$ / $FC_{EEG-\beta}$ and FC_{fMRI} may suggest that phase synchrony in α- and β-band contribute particularly strongly to the intrinsic network organization of the brain first characterized in FC_{fMRI}, paralleling conclusions of prior MEG studies (Brookes et al., 2011; Hipp et al., 2012).

This conclusion may come as a surprise, since neurophysiological investigations using intracranial studies (human or animal) have demonstrated highest correlation between local BOLD amplitudes and γ power (Logothetis et al., 2001; Nir et al., 2007). In this context, it is important keep in mind the difference between local signal amplitudes and whole-brain FC organization. Further, we note that beyond $FC_{EEG-\alpha/\beta}$ we found weaker but significant correlations between FC_{fMRI} and $FC_{EEG-\gamma}$ (as well as $FC_{EEG-\delta}$) for all connectivity measures with the exception of FC_{fMRI}-$FC_{EEG-\gamma}$ correlation in the 256Ch-3T dataset when using orthogonalized amplitude envelope correlations (AEC) (see also section Low SNR of gamma).

Additionally, in our previous work we have shown that local (visual) $FC_{EEG-\gamma}$ as well as distributed $FC_{EEG-\delta}$ provide additional information (beyond $FC_{EEG-\alpha}$ and $FC_{EEG-\beta}$) to explain structural connectivity derived from dMRI (Wirsich et al., 2017). Further, we recently demonstrated that $FC_{EEG-\gamma}$ provides spatially independent information to the FC_{fMRI}-FC_{EEG} relationship (Wirsich et al., 2020a). A frequency specific crossmodal relationship is further to be expected from the laminar organization of the brain linking EEG-γ activity to local laminar connectivity while lower frequencies support long range projections (Scheeringa et al., 2016; Scheeringa and Fries, 2017). To conclude, $FC_{EEG-\gamma}$ meaningfully and uniquely relates to FC_{fMRI} albeit at a weaker effect size.

Spatial contributions and ICN organization across timescales

We observed that ICNs in general and particularly the visual and limbic network consistently contributed more to the static crossmodal correlation across all frequency bands. Intra-ICN connections do not only have the highest connectivity but were also previously found to have the least dynamic connections in the brain (Zalesky et al., 2014). Together with our results this suggests the existence of a crossmodal static core component present in both EEG and fMRI (Sadaghiani and Wirsich, 2020) potentially mediated by the structural core of the brain (van den Heuvel and Sporns, 2011; Wirsich et al., 2017). This idea of a crossmodal core is further strengthened by the observation of a dominance of homotopic connections to the relationship, in line with (Shen et al., 2015) showing that homotopic regions are among the least dynamic connections of FC_{fMRI}. In the current study we extend these results of (Shen et al., 2015; Wirsich et al., 2020a; Zalesky et al., 2014) by showing that visual, limbic (temporo-orbitofrontal) and homotopic connections are the largest contributors to the static crossmodal FC_{fMRI}-FC_{EEG} relationship. If this property would be only driven by SNR of the EEG signal, we would expect that $FC_{EEG-\beta}$ performs equally well when comparing the here presented results to the dynamic crossmodal relationship. As we demonstrated recently (Wirsich et al., 2020b) this is not the case: the dynamic crossmodal relationship is dominated by long-range intra-ICN $FC_{EEG-\delta}$, suggesting different frequency specific crossmodal relationships between EEG and fMRI. Taken together, this suggests a static FC_{fMRI} core dominated by correlation to $FC_{EEG-\beta}$ while the results of Wirsich et al. (2020b) suggest a tight link of long-range dynamic $FC_{EEG-\delta}$ linked to dynamic FC_{fMRI}.

The relationship between FC_{fMRI} and FC_{EEG} derived by imaginary part of coherency and amplitude envelope correlation

We confirmed that correlation of amplitude envelope correlations (AEC) are related to fMRI (Deligianni et al., 2014) and provide consistent, reliable estimates of connectivity (Colclough et al., 2016). While $AEC_{non\text{-}orthogonalized}$ correlated the most to FC_{fMRI}, it has been noted that this cross-measure consistency might stem from source leakage. It has been proposed that source leakage can be solved by orthogonalization of the signal pairs before calculating the AEC (Colclough et al., 2016). Colclough et al. (2016) observed a poorer (inter- and intrasubject) reliability of coherence-based measures as compared to AEC. Exploring the FC_{EEG}-FC_{fMRI} correlation across datasets, we observed that the imaginary part of the coherency had a higher crossmodal correlation than $AEC_{orthogonalized}$ but lower crossmodal correlation when compared to $AEC_{non\text{-}orthogonalized}$. As we observed higher correlation of AEC-based FC_{EEG} with FC_{fMRI} when not using orthogonalization, it might be the case that the orthogonalization eliminates true FC_{EEG} correlated to FC_{fMRI}. Instead of orthogonalization Glomb et al. (2020) proposed to filter the FC_{EEG} using structural connectivity derived by dMRI. In that sense it could be argued that $AEC_{non\text{-}orthogonalized}$ provides the best measure as it has been shown to be both the most reliable measure of FC_{EEG} (Colclough et al., 2016) and to have a higher crossmodal correlation to FC_{fMRI} as compared to iCoh and $AEC_{orthognalized}$ (Fig

3). Further work is needed to better understand the contribution of veridic neuronal connectivity at zero lag (Engel et al., 1991) that is suppressed by either using orthogonalization or imaginary part of the coherency. As the reliability of imaginary part of the coherency in terms of high FC_{EEG}-FC_{fMRI} crossmodal correlation falls between orthogonalized and non-orthognalized AEC we conclude that our results provide further evidence for the overall concordance of amplitude-based and phase-based static connectivity (Mostame and Sadaghiani, 2020; Sadaghiani and Wirsich, 2020). Beyond the measurement of undirected connectivity, EEG has been shown to be able to extract the directional connectivity of ICN organization (Coito et al., 2019) and ultimately a multimodal approach holds the promise to better estimate effective connectivity (Wei et al., 2020).

Crossmodal correlation of high-quality EEG-fMRI connectomes at 7T

Here we demonstrated for the first time that simultaneous EEG-fMRI connectivity estimation can be undertaken at 7T, providing reliable monomodal estimates of FC_{fMRI} and FC_{EEG} comparable to data at 3T and 1.5T. EEG connectomes remain generally reliable at 64Ch-7T when compared to the other datasets (inter-dataset correlation of FC_{EEG}: r>0.51 vs. r>0.43 for all other datasets, Table 2). This is despite the increased interferences between the two modalities at 7T (Debener et al., 2008; Jorge et al., 2015b; Mullinger et al., 2008b). We controlled for EEG artifacts by using the artifact acquisition approach of Jorge et al. (2015a) recording 4 electrodes isolated from the scalp to improve data quality. Opposed to that, for fMRI we measured a lower correlation of FC_{fMRI} between the 64Ch-7T dataset and the other datasets (r>0.64 vs. r>0.78 for non-7T datasets, Table 1). This is most likely due to artifacts induced on the fMRI by strong influence of the EEG leads converging to the superior-parietal regions of the cap (Jorge et al., 2015b). This artifact can potentially be avoided by customizing the cabling of the EEG cap (Meyer et al., 2019) and future studies should investigate the effects on FC_{fMRI} of this improvement.

The impact of the number of EEG channels and cortical regions

In line with previous work we confirm that monomodal and cross modal reliability was not increased when adding more than 64 channels (Lantz et al., 2003). Related, the optimal number of distinguishable regions (in terms of cross talk between source reconstructed M/EEG signals) to be used in source reconstruction was found to be around 70 regions (Farahibozorg et al., 2018), both for MEG (204 planar gradiometers, 102 magnetometers) and EEG (70 channels). Consequently, our expectation was not that 256 channels will perform much better than 64 channels. Surprisingly, we found that the 256 channel EEG setup performed the lowest with a higher resolution atlas (Fig 2b) and when estimating single subject estimates of the FC_{EEG}-FC_{fMRI} correlation (Table 4). Those results should be interpreted with caution as the 256 channels system comes with a different setup (long 2m cable from amplifier to cap (Iannotti et al., 2015)). It has been demonstrated that a longer cable length to the amplifier negatively affects the EEG data quality inside the scanner (especially high frequencies such as the gamma band (Jorge et al., 2015b)). Additionally, the electrode/sponge/amplifier system used in the 256 channel setup has generally higher impedances of individual electrodes (e.g. (Foged et al., 2017) used impedance limits of <20kΩ for a 64 electrode electrode/gel system and <50kΩ for the 256 channel electrode/sponge system). Future work should investigate FC_{EEG} as a function of using 64 or 256 electrodes outside the MR-scanner room.

Low SNR of gamma and the impact of artifacts specific to EEG inside a scanner

Due to the limitation of recording the electrophysiological signal at the scalp, EEG high-γ frequencies (>60Hz) are discarded for analysis. But even the low-γ range from 30-60Hz has been shown to be

difficult to analyze in a simultaneous EEG-fMRI setup (Uji et al., 2018). Due to its lower signal power, the EEG-γ band is most affected by a range of different sources of scanner-related artifacts (Jorge et al., 2015b; Uji et al., 2018). As EEG artifacts increase as a function of field strength (Debener et al., 2008), the 64Ch-1.5T performed by far the best in terms of FC_{fMRI}-$FC_{EEG-\gamma}$ correlation (this is despite the drop in BOLD sensitivity, see Table 1). Additionally the EEG-γ SNR seems to be particularly decreased by long cables (EEG cap to EEG amplifiers) (Jorge et al., 2015b) and vibration artifacts due to the scanner's helium pump (Jorge et al., 2015b; Nierhaus et al., 2013; Rothlübbers et al., 2015). This is highlighted by our results of the 256Ch-3T setup with longer cables and with the helium pump turned on which might have caused the additional decrease of $FC_{EEG-\gamma}$ correlations. An alternative to using low field strength was recently proposed with the use of fast multiband sequences with a fast TR followed by a 'silent' period with no scanning to extract the gamma signal (Uji et al., 2018). As another approach to further correct for EEG artifacts in the scanner the use of electrodes as motion artifact sensors (Jorge et al., 2015a; Masterton et al., 2007) has been proposed to monitor all magnetic induction effects such as gradient, pulse-related (or cardioballistic), vibration and spontaneous motion. Iannotti et al. (2015) proposed a similar approach using cheek electrodes (with less/no neuronal signal) to better estimate the pulse artefact. We demonstrate in our 64Ch-7T data that the motion sensor approach can help to generate reliable FC_{EEG} even in an artifact-sensitive ultra-high-field scanner setting. Our correction technique used in the 64Ch-7T dataset may have greatly contributed for $FC_{EEG-\gamma}$ being most correlated to the less artifactual $FC_{EEG-\gamma}$ recorded in the 1.5T scanner (as compared to the two 3T datasets, Table 2) and FC_{fMRI} - $FC_{EEG-\gamma}$ correlations being higher than in the 64Ch-3T and 256Ch-3T datasets (Fig 2).

Further methodological considerations and future work

The goal of this study was not to perfectly control for all acquisition and preprocessing steps but to assess the generalizability and reliability in a heterogenous setting, representative of the variability of center specific protocols (Botvinik-Nezer et al., 2020). The reliable results of the general correlation between EEG and fMRI connectivity confirm the feasibility of using this approach in multicentric settings.

Though brain-wide changes (largest effect size in visual areas) of FC_{fMRI} have been reported between eyes-open and eyes-closed conditions (Agcaoglu et al., 2019), both conditions are discussed interchangeably for FC_{fMRI} in the literature (Buckner et al., 2013) and we did not find any systematic changes between conditions (SI results). A general stability of ICNs across conditions is also supported by the finding that ICNs are not only observable during rest but also while performing a task (Cole et al., 2014; Krienen et al., 2014). Future work may study this aspect more specifically by recording both eyes-open and eyes-closed data in the same subjects with one specific EEG-fMRI setup. Equally, alertness and wakefulness have been shown to further confound FC analysis (Tagliazucchi and Laufs, 2014).

Besides the variability induced by different hardware setups especially for EEG (Pernet et al., 2019), source analysis (Mahjoory et al., 2017) and connectivity estimation (Colclough et al., 2016) provide more heterogenous analysis options than the more consolidated field of fMRI processing. Better controlling the variable outcome of complex processing pipelines is needed (Botvinik-Nezer et al., 2020; Carp, 2012). Guidelines might recommend specific steps and strategies of best practice to improve neurobiological relevance and reduce erroneous localization/connections (He et al., 2019).

Conclusion

In conclusion, we demonstrated the reliability of EEG-fMRI connectomes across various acquisition setups and established for the first time the feasibility of extracting reliable EEG-fMRI connectomes at 7T. From a fMRI perspective, the intrinsic connectivity organization of the brain has been linked both to cognitive states and pathology. Reliable estimation of crossmodal network organization adds a new dimension of how we can assess the healthy and pathologic brain, by dissociating the neurobiological scenarios that may give rise to the observed similarity of FC organization across timescales and modalities.

Acknowledgements

We thank Katia Lehongre, Benjamin Morillon (64Ch-3T dataset) and Fani Deligianni and Jonathan Clayden (64Ch-1.5T dataset) for generously sharing their data. SV, JW and FG acknowledge support from Swiss National Science Foundation (SNSF, under grants CRSII5_170873, 169198 and 192749 to SG, JW and 188769 to FG). SS acknowledges financial support from NIH R01MH11622601A1 and R21NS10460302. ALG was supported by ERC 260347 – COMPUSLANG. JJ and RG were supported by Centre d'Imagerie BioMédicale (CIBM) of the UNIL, UNIGE, HUG, CHUV, EPFL and the Leenaards and Jeantet Foundations.

Bibliography

Abreu, R., Leal, A., Figueiredo, P., 2018. EEG-Informed fMRI: A Review of Data Analysis Methods. Front. Hum. Neurosci. 12. https://doi.org/10.3389/fnhum.2018.00029

Abreu, R., Leite, M., Jorge, J., Grouiller, F., van der Zwaag, W., Leal, A., Figueiredo, P., 2016. Ballistocardiogram artifact correction taking into account physiological signal preservation in simultaneous EEG-fMRI. NeuroImage 135, 45–63. https://doi.org/10.1016/j.neuroimage.2016.03.034

Abreu, R., Simões, M., Castelo-Branco, M., 2020. Pushing the Limits of EEG: Estimation of Large-Scale Functional Brain Networks and Their Dynamics Validated by Simultaneous fMRI. Front. Neurosci. 14. https://doi.org/10.3389/fnins.2020.00323

Agcaoglu, O., Wilson, T.W., Wang, Y.-P., Stephen, J., Calhoun, V.D., 2019. Resting state connectivity differences in eyes open versus eyes closed conditions. Hum. Brain Mapp. 40, 2488–2498. https://doi.org/10.1002/hbm.24539

Allen, P.J., Josephs, O., Turner, R., 2000. A method for removing imaging artifact from continuous EEG recorded during functional MRI. Neuroimage 12, 230–239. https://doi.org/10.1006/nimg.2000.0599

Allen, P.J., Polizzi, G., Krakow, K., Fish, D.R., Lemieux, L., 1998. Identification of EEG events in the MR scanner: the problem of pulse artifact and a method for its subtraction. Neuroimage 8, 229–239. https://doi.org/10.1006/nimg.1998.0361

Amico, E., Goñi, J., 2018. The quest for identifiability in human functional connectomes. Sci. Rep. 8, 1–14. https://doi.org/10.1038/s41598-018-25089-1

Amico, E., Marinazzo, D., Di Perri, C., Heine, L., Annen, J., Martial, C., Dzemidzic, M., Kirsch, M., Bonhomme, V., Laureys, S., Goñi, J., 2017. Mapping the functional connectome traits of levels of consciousness. NeuroImage 148, 201–211. https://doi.org/10.1016/j.neuroimage.2017.01.020

Andersson, J.L.R., Skare, S., Ashburner, J., 2003. How to correct susceptibility distortions in spin-echo echo-planar images: application to diffusion tensor imaging. NeuroImage 20, 870–888. https://doi.org/10.1016/S1053-8119(03)00336-7

Avants, B.B., Tustison, N.J., Wu, J., Cook, P.A., Gee, J.C., 2011. An open source multivariate framework for n-tissue segmentation with evaluation on public data. Neuroinformatics 9, 381–400. https://doi.org/10.1007/s12021-011-9109-y

Badhwar, A., Collin-Verreault, Y., Orban, P., Urchs, S., Chouinard, I., Vogel, J., Potvin, O., Duchesne, S., Bellec, P., 2020. Multivariate consistency of resting-state fMRI connectivity maps acquired on a single individual over 2.5 years, 13 sites and 3 vendors. NeuroImage 205, 116210. https://doi.org/10.1016/j.neuroimage.2019.116210

Baillet, S., Mosher, J.C., Leahy, R.M., 2001. Electromagnetic brain mapping. IEEE Signal Process. Mag. 18, 14–30. https://doi.org/10.1109/79.962275

Bell, A.J., Sejnowski, T.J., 1995. An information-maximization approach to blind separation and blind deconvolution. Neural Comput 7, 1129–1159.

Biswal, B., Yetkin, F.Z., Haughton, V.M., Hyde, J.S., 1995. Functional connectivity in the motor cortex of resting human brain using echo-planar MRI. Magn. Reson. Med. 34, 537–541.

Botvinik-Nezer, R., Holzmeister, F., Camerer, C.F., Dreber, A., Huber, J., Johannesson, M., Kirchler, M., Iwanir, R., Mumford, J.A., Adcock, R.A., Avesani, P., Baczkowski, B.M., Bajracharya, A., Bakst, L., Ball, S., Barilari, M., Bault, N., Beaton, D., Beitner, J., Benoit, R.G., Berkers, R.M.W.J., Bhanji, J.P., Biswal, B.B., Bobadilla-Suarez, S., Bortolini, T., Bottenhorn, K.L., Bowring, A., Braem, S., Brooks, H.R., Brudner, E.G., Calderon, C.B., Camilleri, J.A., Castrellon, J.J., Cecchetti, L., Cieslik, E.C., Cole, Z.J., Collignon, O., Cox, R.W., Cunningham, W.A., Czoschke, S., Dadi, K., Davis, C.P., Luca, A.D., Delgado, M.R., Demetriou, L., Dennison, J.B., Di, X., Dickie, E.W., Dobryakova, E., Donnat, C.L., Dukart, J., Duncan, N.W., Durnez, J., Eed, A., Eickhoff, S.B., Erhart, A., Fontanesi, L., Fricke, G.M., Fu, S., Galván, A., Gau, R., Genon, S., Glatard, T., Glerean, E., Goeman, J.J., Golowin, S.A.E., González-García, C., Gorgolewski, K.J., Grady, C.L., Green, M.A., Guassi Moreira, J.F., Guest, O., Hakimi, S., Hamilton, J.P., Hancock, R., Handjaras, G., Harry, B.B., Hawco, C., Herholz, P., Herman, G., Heunis, S., Hoffstaedter, F., Hogeveen, J., Holmes, S., Hu, C.-P., Huettel, S.A., Hughes, M.E., Iacovella, V., Iordan, A.D., Isager, P.M., Isik, A.I., Jahn, A., Johnson, M.R., Johnstone, T., Joseph, M.J.E., Juliano, A.C., Kable, J.W., Kassinopoulos, M., Koba, C., Kong, X.-Z., Koscik, T.R., Kucukboyaci, N.E., Kuhl, B.A., Kupek, S., Laird, A.R., Lamm, C., Langner, R., Lauharatanahirun, N., Lee, H., Lee, S., Leemans, A., Leo, A., Lesage, E., Li, F., Li, M.Y.C., Lim, P.C., Lintz, E.N., Liphardt, S.W., Losecaat Vermeer, A.B., Love, B.C., Mack, M.L., Malpica, N., Marins, T., Maumet, C., McDonald, K., McGuire, J.T., Melero, H., Méndez Leal, A.S., Meyer, B., Meyer, K.N., Mihai, G., Mitsis, G.D., Moll, J., Nielson, D.M., Nilsonne, G., Notter, M.P., Olivetti, E., Onicas, A.I., Papale, P., Patil, K.R., Peelle, J.E., Pérez, A., Pischedda, D., Poline, J.-B., Prystauka, Y., Ray, S., Reuter-Lorenz, P.A., Reynolds, R.C., Ricciardi, E., Rieck, J.R., Rodriguez-Thompson, A.M., Romyn, A., Salo, T., Samanez-Larkin, G.R., Sanz-Morales, E., Schlichting, M.L., Schultz, D.H., Shen, Q., Sheridan, M.A., Silvers, J.A., Skagerlund, K., Smith, A., Smith, D.V., Sokol-Hessner, P., Steinkamp, S.R., Tashjian, S.M., Thirion, B., Thorp, J.N., Tinghög, G., Tisdall, L., Tompson, S.H., Toro-Serey, C., Torre Tresols, J.J., Tozzi, L., Truong, V., Turella, L., van 't Veer, A.E., Verguts, T., Vettel, J.M., Vijayarajah, S., Vo, K., Wall, M.B., Weeda, W.D., Weis, S., White, D.J., Wisniewski, D., Xifra-Porxas, A., Yearling, E.A., Yoon, S., Yuan, R., Yuen, K.S.L., Zhang, L., Zhang, X., Zosky, J.E., Nichols, T.E., Poldrack, R.A., Schonberg, T., 2020. Variability in the analysis of a single neuroimaging dataset by many teams. Nature 1–7. https://doi.org/10.1038/s41586-020-2314-9

Brookes, M.J., Woolrich, M., Luckhoo, H., Price, D., Hale, J.R., Stephenson, M.C., Barnes, G.R., Smith, S.M., Morris, P.G., 2011. Investigating the electrophysiological basis of resting state networks using magnetoencephalography. Proc. Natl. Acad. Sci. 108, 16783–16788. https://doi.org/10.1073/pnas.1112685108

Brookes, M.J., Woolrich, M.W., Barnes, G.R., 2012. Measuring functional connectivity in MEG: A multivariate approach insensitive to linear source leakage. NeuroImage 63, 910–920. https://doi.org/10.1016/j.neuroimage.2012.03.048

Buckner, R.L., Krienen, F.M., Yeo, B.T.T., 2013. Opportunities and limitations of intrinsic functional connectivity MRI. Nat. Neurosci. 16, 832–837. https://doi.org/10.1038/nn.3423

Carp, J., 2012. On the plurality of (methodological) worlds: estimating the analytic flexibility of FMRI experiments. Front. Neurosci. 6, 149. https://doi.org/10.3389/fnins.2012.00149

Chu, C.J., Tanaka, N., Diaz, J., Edlow, B.L., Wu, O., Hämäläinen, M., Stufflebeam, S., Cash, S.S., Kramer, M.A., 2015. EEG functional connectivity is partially predicted by underlying white matter connectivity. NeuroImage 108, 23–33. https://doi.org/10.1016/j.neuroimage.2014.12.033

Coito, A., Michel, C.M., Vulliemoz, S., Plomp, G., 2019. Directed functional connections underlying spontaneous brain activity. Hum. Brain Mapp. 40, 879–888. https://doi.org/10.1002/hbm.24418

Colclough, G.L., Woolrich, M.W., Tewarie, P.K., Brookes, M.J., Quinn, A.J., Smith, S.M., 2016. How reliable are MEG resting-state connectivity metrics? NeuroImage 138, 284–293. https://doi.org/10.1016/j.neuroimage.2016.05.070

Cole, M.W., Bassett, D.S., Power, J.D., Braver, T.S., Petersen, S.E., 2014. Intrinsic and task-evoked network architectures of the human brain. Neuron 83, 238–251. https://doi.org/10.1016/j.neuron.2014.05.014

Coquelet, N., De Tiège, X., Destoky, F., Roshchupkina, L., Bourguignon, M., Goldman, S., Peigneux, P., Wens, V., 2020. Comparing MEG and high-density EEG for intrinsic functional connectivity mapping. NeuroImage 210, 116556. https://doi.org/10.1016/j.neuroimage.2020.116556

de Pasquale, F., Della Penna, S., Snyder, A.Z., Lewis, C., Mantini, D., Marzetti, L., Belardinelli, P., Ciancetta, L., Pizzella, V., Romani, G.L., Corbetta, M., 2010. Temporal dynamics of spontaneous MEG activity in brain networks. Proc. Natl. Acad. Sci. U. S. A. 107, 6040–6045. https://doi.org/10.1073/pnas.0913863107

De Vico Fallani, F., Richiardi, J., Chavez, M., Achard, S., 2014. Graph analysis of functional brain networks: practical issues in translational neuroscience. Philos. Trans. R. Soc. Lond. B. Biol. Sci. 369. https://doi.org/10.1098/rstb.2013.0521

Debener, S., Mullinger, K.J., Niazy, R.K., Bowtell, R.W., 2008. Properties of the ballistocardiogram artefact as revealed by EEG recordings at 1.5, 3 and 7 T static magnetic field strength. Int. J. Psychophysiol., Integration of EEG and fMRI 67, 189–199. https://doi.org/10.1016/j.ijpsycho.2007.05.015

Deligianni, F., Carmichael, D.W., Zhang, G.H., Clark, C.A., Clayden, J.D., 2016. NODDI and Tensor-Based Microstructural Indices as Predictors of Functional Connectivity. PLOS ONE 11, e0153404. https://doi.org/10.1371/journal.pone.0153404

Deligianni, F., Centeno, M., Carmichael, D.W., Clayden, J.D., 2014. Relating resting-state fMRI and EEG whole-brain connectomes across frequency bands. Front. Neurosci. 8. https://doi.org/10.3389/fnins.2014.00258

Deligianni, F., Clayden, J., Yang, G.-Z., 2019. Comparison of Brain Networks Based on Predictive Models of Connectivity, in: 2019 IEEE 19th International Conference on Bioinformatics and Bioengineering (BIBE). Presented at the 2019 IEEE 19th International Conference on Bioinformatics and Bioengineering (BIBE), pp. 115–121. https://doi.org/10.1109/BIBE.2019.00029

Delorme, A., Makeig, S., 2004. EEGLAB: an open source toolbox for analysis of single-trial EEG dynamics including independent component analysis. J. Neurosci. Methods 134, 9–21. https://doi.org/10.1016/j.jneumeth.2003.10.009

de Pasquale, F., Della Penna, S., Snyder, A.Z., Marzetti, L., Pizzella, V., Romani, G.L., Corbetta, M., 2012. A Cortical Core for Dynamic Integration of Functional Networks in the Resting Human Brain. Neuron 74, 753–764. https://doi.org/10.1016/j.neuron.2012.03.031

Desikan, R.S., Ségonne, F., Fischl, B., Quinn, B.T., Dickerson, B.C., Blacker, D., Buckner, R.L., Dale, A.M., Maguire, R.P., Hyman, B.T., Albert, M.S., Killiany, R.J., 2006. An automated labeling system for subdividing the human cerebral cortex on MRI scans into gyral based regions of interest. NeuroImage 31, 968–980. https://doi.org/10.1016/j.neuroimage.2006.01.021

Engel, A.K., Gerloff, C., Hilgetag, C.C., Nolte, G., 2013. Intrinsic Coupling Modes: Multiscale Interactions in Ongoing Brain Activity. Neuron 80, 867–886. https://doi.org/10.1016/j.neuron.2013.09.038

Engel, A.K., Kreiter, A.K., König, P., Singer, W., 1991. Synchronization of oscillatory neuronal responses between striate and extrastriate visual cortical areas of the cat. Proc. Natl. Acad. Sci. U. S. A. 88, 6048–6052.

Farahibozorg, S.-R., Henson, R.N., Hauk, O., 2018. Adaptive cortical parcellations for source reconstructed EEG/MEG connectomes. NeuroImage 169, 23–45. https://doi.org/10.1016/j.neuroimage.2017.09.009

Finger, H., Bönstrup, M., Cheng, B., Messé, A., Hilgetag, C., Thomalla, G., Gerloff, C., König, P., 2016. Modeling of Large-Scale Functional Brain Networks Based on Structural Connectivity from DTI: Comparison with EEG Derived Phase Coupling Networks and Evaluation of Alternative Methods along the Modeling Path. PLOS Comput Biol 12, e1005025. https://doi.org/10.1371/journal.pcbi.1005025

Finn, E.S., Shen, X., Scheinost, D., Rosenberg, M.D., Huang, J., Chun, M.M., Papademetris, X., Constable, R.T., 2015. Functional connectome fingerprinting: identifying individuals using patterns of brain connectivity. Nat. Neurosci. advance online publication. https://doi.org/10.1038/nn.4135

Foged, M.T., Lindberg, U., Vakamudi, K., Larsson, H.B.W., Pinborg, L.H., Kjær, T.W., Fabricius, M., Svarer, C., Ozenne, B., Thomsen, C., Beniczky, S., Paulson, O.B., Posse, S., 2017. Safety and EEG data quality of concurrent high-density EEG and high-speed fMRI at 3 Tesla. PLoS ONE 12. https://doi.org/10.1371/journal.pone.0178409

Fox, M.D., Snyder, A.Z., Vincent, J.L., Corbetta, M., Essen, D.C.V., Raichle, M.E., 2005. The human brain is intrinsically organized into dynamic, anticorrelated functional networks. Proc. Natl. Acad. Sci. U. S. A. 102, 9673–9678. https://doi.org/10.1073/pnas.0504136102

Glomb, K., Mullier, E., Carboni, M., Rubega, M., Iannotti, G., Tourbier, S., Seeber, M., Vulliemoz, S., Hagmann, P., 2020. Using structural connectivity to augment community structure in EEG functional connectivity. Netw. Neurosci. 1–59. https://doi.org/10.1162/netn_a_00147

Gonçalves, S.I., Pouwels, P.J.W., Kuijer, J.P.A., Heethaar, R.M., de Munck, J.C., 2007. Artifact removal in co-registered EEG/fMRI by selective average subtraction. Clin. Neurophysiol. Off. J. Int. Fed. Clin. Neurophysiol. 118, 2437–2450. https://doi.org/10.1016/j.clinph.2007.08.017

Gramfort, A., Papadopoulo, T., Olivi, E., Clerc, M., 2010. OpenMEEG: opensource software for quasistatic bioelectromagnetics. Biomed. Eng. OnLine 9, 45. https://doi.org/10.1186/1475-925X-9-45

Greicius, M.D., Krasnow, B., Reiss, A.L., Menon, V., 2003. Functional connectivity in the resting brain: a network analysis of the default mode hypothesis. Proc. Natl. Acad. Sci. U. S. A. 100, 253–258. https://doi.org/10.1073/pnas.0135058100

Han, X., Jovicich, J., Salat, D., van der Kouwe, A., Quinn, B., Czanner, S., Busa, E., Pacheco, J., Albert, M., Killiany, R., Maguire, P., Rosas, D., Makris, N., Dale, A., Dickerson, B., Fischl, B., 2006. Reliability of MRI-derived measurements of human cerebral cortical thickness: the effects of field strength, scanner upgrade and manufacturer. NeuroImage 32, 180–194. https://doi.org/10.1016/j.neuroimage.2006.02.051

He, B., Astolfi, L., Valdes-Sosa, P.A., Marinazzo, D., Palva, S., Benar, C.G., Michel, C.M., Koenig, T., 2019. Electrophysiological Brain Connectivity: Theory and Implementation. IEEE Trans. Biomed. Eng. 1–1. https://doi.org/10.1109/TBME.2019.2913928

Hipp, J.F., Hawellek, D.J., Corbetta, M., Siegel, M., Engel, A.K., 2012. Large-scale cortical correlation structure of spontaneous oscillatory activity. Nat. Neurosci. 15. https://doi.org/10.1038/nn.3101

Hipp, J.F., Siegel, M., 2015. BOLD fMRI Correlation Reflects Frequency-Specific Neuronal Correlation. Curr. Biol. 25, 1368–1374. https://doi.org/10.1016/j.cub.2015.03.049

Honey, C.J., Sporns, O., Cammoun, L., Gigandet, X., Thiran, J.P., Meuli, R., Hagmann, P., 2009. Predicting human resting-state functional connectivity from structural connectivity. Proc. Natl. Acad. Sci. 106, 2035–2040. https://doi.org/10.1073/pnas.0811168106

Iannotti, G.R., Pittau, F., Michel, C.M., Vulliemoz, S., Grouiller, F., 2015. Pulse Artifact Detection in Simultaneous EEG–fMRI Recording Based on EEG Map Topography. Brain Topogr. 28, 21–32. https://doi.org/10.1007/s10548-014-0409-z

Jenkinson, M., Bannister, P., Brady, M., Smith, S., 2002. Improved optimization for the robust and accurate linear registration and motion correction of brain images. NeuroImage 17, 825–841. https://doi.org/10.1016/s1053-8119(02)91132-8

Jenkinson, M., Smith, S., 2001. A global optimisation method for robust affine registration of brain images. Med. Image Anal. 5, 143–156. https://doi.org/10.1016/s1361-8415(01)00036-6

Jorge, J., Bouloc, C., Bréchet, L., Michel, C.M., Gruetter, R., 2019. Investigating the variability of cardiac pulse artifacts across heartbeats in simultaneous EEG-fMRI recordings: A 7T study. NeuroImage 191, 21–35. https://doi.org/10.1016/j.neuroimage.2019.02.021

Jorge, J., Figueiredo, P., Gruetter, R., van der Zwaag, W., 2018. Mapping and characterization of positive and negative BOLD responses to visual stimulation in multiple brain regions at 7T. Hum. Brain Mapp. 39, 2426–2441. https://doi.org/10.1002/hbm.24012

Jorge, J., Grouiller, F., Gruetter, R., van der Zwaag, W., Figueiredo, P., 2015a. Towards high-quality simultaneous EEG-fMRI at 7T: Detection and reduction of EEG artifacts due to head motion. NeuroImage 120, 143–153. https://doi.org/10.1016/j.neuroimage.2015.07.020

Jorge, J., Grouiller, F., Ipek, Ö., Stoermer, R., Michel, C.M., Figueiredo, P., van der Zwaag, W., Gruetter, R., 2015b. Simultaneous EEG-fMRI at ultra-high field: artifact prevention and safety assessment. NeuroImage 105, 132–144. https://doi.org/10.1016/j.neuroimage.2014.10.055

Krienen, F.M., Yeo, B.T.T., Buckner, R.L., 2014. Reconfigurable task-dependent functional coupling modes cluster around a core functional architecture. Philos. Trans. R. Soc. Lond. B. Biol. Sci. 369. https://doi.org/10.1098/rstb.2013.0526

Kybic, J., Clerc, M., Abboud, T., Faugeras, O., Keriven, R., Papadopoulo, T., 2005. A common formalism for the Integral formulations of the forward EEG problem. IEEE Trans. Med. Imaging 24, 12–28. https://doi.org/10.1109/TMI.2004.837363

Lantz, G., Grave de Peralta, R., Spinelli, L., Seeck, M., Michel, C.M., 2003. Epileptic source localization with high density EEG: how many electrodes are needed? Clin. Neurophysiol. Off. J. Int. Fed. Clin. Neurophysiol. 114, 63–69. https://doi.org/10.1016/s1388-2457(02)00337-1

Logothetis, N.K., Pauls, J., Augath, M., Trinath, T., Oeltermann, A., 2001. Neurophysiological investigation of the basis of the fMRI signal. Nature 412, 150–157. https://doi.org/10.1038/35084005

Mahjoory, K., Nikulin, V.V., Botrel, L., Linkenkaer-Hansen, K., Fato, M.M., Haufe, S., 2017. Consistency of EEG source localization and connectivity estimates. NeuroImage 152, 590–601. https://doi.org/10.1016/j.neuroimage.2017.02.076

Mandelkow, H., Halder, P., Boesiger, P., Brandeis, D., 2006. Synchronization facilitates removal of MRI artefacts from concurrent EEG recordings and increases usable bandwidth. NeuroImage 32, 1120–1126. https://doi.org/10.1016/j.neuroimage.2006.04.231

Marquetand, J., Vannoni, S., Carboni, M., Li Hegner, Y., Stier, C., Braun, C., Focke, N.K., 2019. Reliability of Magnetoencephalography and High-Density Electroencephalography Resting-State Functional Connectivity Metrics. Brain Connect. https://doi.org/10.1089/brain.2019.0662

Masterton, R.A.J., Abbott, D.F., Fleming, S.W., Jackson, G.D., 2007. Measurement and reduction of motion and ballistocardiogram artefacts from simultaneous EEG and fMRI recordings. NeuroImage 37, 202–211. https://doi.org/10.1016/j.neuroimage.2007.02.060

Meier, J., Tewarie, P., Hillebrand, A., Douw, L., van Dijk, B., Stufflebeam, S., Van Mieghem, P.F.A., 2016. A mapping between structural and functional brain networks. Brain Connect. https://doi.org/10.1089/brain.2015.0408

Meyer, M.C., Scheeringa, R., Webb, A.G., Petridou, N., Kraff, O., Norris, D.G., 2019. Adapted cabling of an EEG cap improves simultaneous measurement of EEG and fMRI at 7T. J. Neurosci. Methods 108518. https://doi.org/10.1016/j.jneumeth.2019.108518

Mo, J., Liu, Y., Huang, H., Ding, M., 2013. Coupling between Visual Alpha Oscillations and Default Mode Activity. NeuroImage 68, 112–118. https://doi.org/10.1016/j.neuroimage.2012.11.058

Morillon, B., Lehongre, K., Frackowiak, R.S.J., Ducorps, A., Kleinschmidt, A., Poeppel, D., Giraud, A.-L., 2010. Neurophysiological origin of human brain asymmetry for speech and language. Proc. Natl. Acad. Sci. 107, 18688–18693. https://doi.org/10.1073/pnas.1007189107

Mostame, P., Sadaghiani, S., 2020. Phase- and amplitude-coupling are tied by an intrinsic spatial organization but show divergent stimulus-related changes. NeuroImage 117051. https://doi.org/10.1016/j.neuroimage.2020.117051

Mullinger, K., Brookes, M., Stevenson, C., Morgan, P., Bowtell, R., 2008a. Exploring the feasibility of simultaneous electroencephalography/functional magnetic resonance imaging at 7 T. Magn. Reson. Imaging 26, 968–977. https://doi.org/10.1016/j.mri.2008.02.014

Mullinger, K., Debener, S., Coxon, R., Bowtell, R., 2008b. Effects of simultaneous EEG recording on MRI data quality at 1.5, 3 and 7 tesla. Int. J. Psychophysiol., Integration of EEG and fMRI 67, 178–188. https://doi.org/10.1016/j.ijpsycho.2007.06.008

Neuner, I., Warbrick, T., Arrubla, J., Felder, J., Celik, A., Reske, M., Boers, F., Shah, N.J., 2013. EEG acquisition in ultra-high static magnetic fields up to 9.4 T. NeuroImage 68, 214–220. https://doi.org/10.1016/j.neuroimage.2012.11.064

Niazy, R.K., Beckmann, C.F., Iannetti, G.D., Brady, J.M., Smith, S.M., 2005. Removal of FMRI environment artifacts from EEG data using optimal basis sets. NeuroImage 28, 720–737. https://doi.org/10.1016/j.neuroimage.2005.06.067

Nierhaus, T., Gundlach, C., Goltz, D., Thiel, S.D., Pleger, B., Villringer, A., 2013. Internal ventilation system of MR scanners induces specific EEG artifact during simultaneous EEG-fMRI. NeuroImage 74, 70–76. https://doi.org/10.1016/j.neuroimage.2013.02.016

Nir, Y., Fisch, L., Mukamel, R., Gelbard-Sagiv, H., Arieli, A., Fried, I., Malach, R., 2007. Coupling between Neuronal Firing Rate, Gamma LFP, and BOLD fMRI Is Related to Interneuronal Correlations. Curr. Biol. 17, 1275–1285. https://doi.org/10.1016/j.cub.2007.06.066

Noble, S., Scheinost, D., Constable, R.T., 2019. A decade of test-retest reliability of functional connectivity: A systematic review and meta-analysis. NeuroImage 203, 116157. https://doi.org/10.1016/j.neuroimage.2019.116157

Nolte, G., Bai, O., Wheaton, L., Mari, Z., Vorbach, S., Hallett, M., 2004. Identifying true brain interaction from EEG data using the imaginary part of coherency. Clin. Neurophysiol. Off. J. Int. Fed. Clin. Neurophysiol. 115, 2292–2307. https://doi.org/10.1016/j.clinph.2004.04.029

Palva, J.M., Wang, S.H., Palva, S., Zhigalov, A., Monto, S., Brookes, M.J., Schoffelen, J.-M., Jerbi, K., 2018. Ghost interactions in MEG/EEG source space: A note of caution on inter-areal coupling measures. NeuroImage 173, 632–643. https://doi.org/10.1016/j.neuroimage.2018.02.032

Pernet, C.R., Appelhoff, S., Gorgolewski, K.J., Flandin, G., Phillips, C., Delorme, A., Oostenveld, R., 2019. EEG-BIDS, an extension to the brain imaging data structure for electroencephalography. Sci. Data 6, 1–5. https://doi.org/10.1038/s41597-019-0104-8

Rothlübbers, S., Relvas, V., Leal, A., Murta, T., Lemieux, L., Figueiredo, P., 2015. Characterisation and reduction of the EEG artefact caused by the helium cooling pump in the MR environment: validation in epilepsy patient data. Brain Topogr. 28, 208–220. https://doi.org/10.1007/s10548-014-0408-0

Sadaghiani, S., Scheeringa, R., Lehongre, K., Morillon, B., Giraud, A.-L., Kleinschmidt, A., 2010. Intrinsic connectivity networks, alpha oscillations, and tonic alertness: a simultaneous electroencephalography/functional magnetic resonance imaging study. J. Neurosci. Off. J. Soc. Neurosci. 30, 10243–10250. https://doi.org/10.1523/JNEUROSCI.1004-10.2010

Sadaghiani, S., Wirsich, J., 2020. Intrinsic connectome organization across temporal scales: New insights from cross-modal approaches. Netw. Neurosci. Camb. Mass 4, 1–29. https://doi.org/10.1162/netn_a_00114

Scheeringa, R., Fries, P., 2017. Cortical layers, rhythms and BOLD signals. NeuroImage. https://doi.org/10.1016/j.neuroimage.2017.11.002

Scheeringa, R., Koopmans, P.J., van Mourik, T., Jensen, O., Norris, D.G., 2016. The relationship between oscillatory EEG activity and the laminar-specific BOLD signal. Proc. Natl. Acad. Sci. U. S. A. 113, 6761–6766. https://doi.org/10.1073/pnas.1522577113

Shen, K., Mišić, B., Cipollini, B.N., Bezgin, G., Buschkuehl, M., Hutchison, R.M., Jaeggi, S.M., Kross, E., Peltier, S.J., Everling, S., Jonides, J., McIntosh, A.R., Berman, M.G., 2015. Stable long-range interhemispheric coordination is supported by direct anatomical projections. Proc. Natl. Acad. Sci. U. S. A. 112, 6473–6478. https://doi.org/10.1073/pnas.1503436112

Siems, M., Siegel, M., 2020. Dissociated neuronal phase- and amplitude-coupling patterns in the human brain. NeuroImage 209, 116538. https://doi.org/10.1016/j.neuroimage.2020.116538

Tadel, F., Baillet, S., Mosher, J.C., Pantazis, D., Leahy, R.M., 2011. Brainstorm: A User-Friendly Application for MEG/EEG Analysis. Comput. Intell. Neurosci. 2011. https://doi.org/10.1155/2011/879716

Tagliazucchi, E., Laufs, H., 2014. Decoding Wakefulness Levels from Typical fMRI Resting-State Data Reveals Reliable Drifts between Wakefulness and Sleep. Neuron 82, 695–708. https://doi.org/10.1016/j.neuron.2014.03.020

Tewarie, P., Bright, M.G., Hillebrand, A., Robson, S.E., Gascoyne, L.E., Morris, P.G., Meier, J., Van Mieghem, P., Brookes, M.J., 2016. Predicting haemodynamic networks using electrophysiology: The role of non-linear and cross-frequency interactions. NeuroImage 130, 273–292. https://doi.org/10.1016/j.neuroimage.2016.01.053

Uji, M., Wilson, R., Francis, S.T., Mullinger, K.J., Mayhew, S.D., 2018. Exploring the advantages of multiband fMRI with simultaneous EEG to investigate coupling between gamma frequency neural activity and the BOLD response in humans. Hum. Brain Mapp. 39, 1673–1687. https://doi.org/10.1002/hbm.23943

van den Heuvel, M.P., Sporns, O., 2011. Rich-Club Organization of the Human Connectome. J. Neurosci. 31, 15775–15786. https://doi.org/10.1523/JNEUROSCI.3539-11.2011

Wei, H., Jafarian, A., Zeidman, P., Litvak, V., Razi, A., Hu, D., Friston, K.J., 2020. Bayesian fusion and multimodal DCM for EEG and fMRI. NeuroImage 211, 116595. https://doi.org/10.1016/j.neuroimage.2020.116595

Wirsich, J., Amico, E., Giraud, A.-L., Goñi, J., Sadaghiani, S., 2020a. Multi-timescale hybrid components of the functional brain connectome: A bimodal EEG-fMRI decomposition. Netw. Neurosci. 1–26. https://doi.org/10.1162/netn_a_00135

Wirsich, J., Giraud, A.-L., Sadaghiani, S., 2020b. Concurrent EEG- and fMRI-derived functional connectomes exhibit linked dynamics. NeuroImage 116998. https://doi.org/10.1016/j.neuroimage.2020.116998

Wirsich, J., Ridley, B., Besson, P., Jirsa, V., Bénar, C., Ranjeva, J.-P., Guye, M., 2017. Complementary contributions of concurrent EEG and fMRI connectivity for predicting structural connectivity. NeuroImage 161, 251–260. https://doi.org/10.1016/j.neuroimage.2017.08.055

Yeo, B.T.T., Krienen, F.M., Sepulcre, J., Sabuncu, M.R., Lashkari, D., Hollinshead, M., Roffman, J.L., Smoller, J.W., Zöllei, L., Polimeni, J.R., Fischl, B., Liu, H., Buckner, R.L., 2011. The organization of the human cerebral cortex estimated by intrinsic functional connectivity. J. Neurophysiol. 106, 1125–1165. https://doi.org/10.1152/jn.00338.2011

Zalesky, A., Fornito, A., Cocchi, L., Gollo, L.L., Breakspear, M., 2014. Time-resolved resting-state brain networks. Proc. Natl. Acad. Sci. 111, 10341–10346. https://doi.org/10.1073/pnas.1400181111

Supplementary Information

	64Ch-1.5T	64Ch-3T	256Ch-3T	64Ch-7T
Subjects				
Number	16	26	21	9
Mean Age	32.41	24.39	32.13	23.56
Paradigm				
Eyes-open/closed	Open	Closed	Closed	Open
Duration	10min48s	30 min	4min58s	8min
Hardware stack				
Scanner	Siemens Avanto	Siemens Tim-Trio	Siemens Magnetom Trio	Siemens Magnetom
TR	2160ms	2000ms	1990ms	1000ms
Helium Pump	Off	Off	On	On
Electrodes	64 (63 active)	64 (62 active)	256 (204 active)	64 (59 active)
Amplifier	Behind the scanner (next to the head of the participant)	Behind the scanner	In front of the scanner (next to the feet of the participant)	Behind the scanner
Impedance	<100kΩ	<20kΩ	<50 kΩ	<20kΩ
Software stack				
Gradient artifact	BrainVisionAnalyser 2	FMRIB	Inhouse (Iannotti et al., 2015)	Inhouse (Jorge et al., 2015a)
Pulse artifact	BrainVisionAnalyser 2	FMRIB	Inhouse (Iannotti et al., 2015)	Inhouse (Jorge et al., 2015a)
ICA cleaning	Yes (BrainVisionAnalyser 2)	No	Yes (EEGLab, runICA v1.29)	Yes (inhouse ICA ext. Infomax algorithm)
Brainstorm	10th August 2017	10th August 2017	15th January 2019	15th January 2019
Freesurfer	v6.0.0	v6.0.0	v6.0.0	v6.0.0
SPM	SPM12 (revision 6906)	SPM12 (revision 6906)	SPM12 (revision 7475)	SPM12 (revision 7475)
FSL	v5.0	v5.0	v5.0	V6.0
ANTs	N/A	N/A	N/A	V2.2.0

SI Table 1: Summary of selected acquisition parameters and data analysis steps

	64Ch-1.5T	64Ch-3T	256Ch-3T	64Ch-7T	All datasets
FC_{fMRI}-$FC_{EEG-\delta}$	11	8	10	8	12
FC_{fMRI}-$FC_{EEG-\theta}$	11	7	10	8	11
FC_{fMRI}-$FC_{EEG-\alpha}$	11	8	9	8	13
FC_{fMRI}-$FC_{EEG-\beta}$	12	8	10	7	11
FC_{fMRI}-$FC_{EEG-\gamma}$	11	9	10	Not stable	15

SI Table 2: The number of subjects needed to generate a stable crossmodal correlation estimate. The stability is assessed by adding a random subject to the average and evaluating the change in crossmodal correlation. The crossmodal correlation is considered stable when the change is not more than 1% of the crossmodal correlation of this frequency band derived from all 72 subjects. Note that for the 64Ch-7T dataset for $FC_{EEG-\gamma}$ no stability was reached when talking all of the 9 subjects.

	64Ch-1.5T	64Ch-3T	256Ch-3T	64Ch-7T	All datasets
β>δ	**0.0002**	0.0102	**0.0002**	0.0074	**<0.0002**
β>θ	0.0014	0.0186	**<0.0002**	0.1706	**<0.0002**
β>α	0.0036	0.0044	0.1918	0.1374	**<0.0002**
β>γ	0.1254	**<0.0002**	**<0.0002**	0.0234	**<0.0002**
α>δ	0.2672	0.6978	0.0022	0.1598	0.0172
α>θ	0.166	0.5862	0.0198	0.6172	0.075
α>γ	0.8546	**0.0002**	**0.0004**	0.6168	0.0084
θ>δ	0.6596	0.6948	0.0044	0.1854	0.0816
θ>γ	0.9662	0.0094	0.0026	0.4862	0.0752
δ>γ	0.951	0.0012	0.023	0.898	0.201

*SI Table 3: P-values of permutation tests comparing the crossmodal FC_{fMRI}-FC_{EEG} correlation between different EEG frequency bands (5000 iterations, Bonferroni-corrected significance level p<0.05 which corresponds to the uncorrected level p<0.05/50 = 0.001, significant cells are marked in **bold**)*

	64Ch-1.5T	64Ch-3T	256Ch-3T	64Ch-7T	All datasets
Desikan>Destrieux					
FC_{fMRI}-$FC_{EEG-\delta}$	0.0068	0.21	0.0036	0.1118	**<0.0002**
FC_{fMRI}-$FC_{EEG-\theta}$	0.0052	0.1012	0.0044	0.0974	**<0.0002**
FC_{fMRI}-$FC_{EEG-\alpha}$	0.0098	0.1392	0.0092	0.068	**<0.0002**
FC_{fMRI}-$FC_{EEG-\beta}$	0.008	0.0688	0.0074	0.139	**<0.0002**
FC_{fMRI}-$FC_{EEG-\gamma}$	0.0068	0.2008	0.0242	0.071	**<0.0002**

*SI Table 4:P-values of permutation tests comparing the crossmodal FC_{fMRI}-FC_{EEG} correlation between different atlases (5000 iterations, Bonferroni-corrected significance level p<0.05 which corresponds to the uncorrected level p<0.05/25 = 0.002, significant cells are marked in **bold**)*

	64Ch-1.5T	64Ch-3T	256Ch-3T	64Ch-7T	All datasets
$AEC_{non-ortho}$ > iCoh					
FC_{fMRI}-$FC_{EEG-\delta}$	0.291	0.0166	**0.0002**	0.1478	0.0016
FC_{fMRI}-$FC_{EEG-\theta}$	0.456	0.283	0.0028	0.5902	0.147
FC_{fMRI}-$FC_{EEG-\alpha}$	0.2088	0.073	0.1134	0.3802	0.0396
FC_{fMRI}-$FC_{EEG-\beta}$	0.2258	0.3366	0.302	0.2994	0.1234
FC_{fMRI}-$FC_{EEG-\gamma}$	0.2698	**<0.0002**	**<0.0002**	0.1178	**<0.0002**
Icoh > AEC_{ortho}					
FC_{fMRI}-$FC_{EEG-\delta}$	0.0026	**<0.0002**	**0.0004**	**<0.0002**	**<0.0002**
FC_{fMRI}-$FC_{EEG-\theta}$	0.069	**<0.0002**	**<0.0002**	0.005	**<0.0002**
FC_{fMRI}-$FC_{EEG-\alpha}$	**0.0012**	**0.0004**	**<0.0002**	0.0022	**<0.0002**
FC_{fMRI}-$FC_{EEG-\beta}$	0.907	**<0.0002**	**<0.0002**	0.0072	**<0.0002**
FC_{fMRI}-$FC_{EEG-\gamma}$	0.0146	0.619	**<0.0002**	0.0112	**<0.0002**

*SI Table 5: P-values of permutation tests comparing the crossmodal FC_{fMRI}-FC_{EEG} correlation between different EEG connectivity measures (5000 iterations, Bonferroni-corrected significance level p<0.05 which corresponds to the uncorrected level p<0.05/50 = 0.001, significant cells are marked in **bold**)*

	64Ch-1.5T	64Ch-3T	256Ch-3T	64Ch-7T	All datasets
All session > 5min					
FC_{fMRI}-$FC_{EEG-\delta}$	0.0472	0.1398		0.73	0.1418
FC_{fMRI}-$FC_{EEG-\theta}$	0.041	0.2178		0.7012	0.132
FC_{fMRI}-$FC_{EEG-\alpha}$	0.1594	0.2748		0.4604	0.2088
FC_{fMRI}-$FC_{EEG-\beta}$	0.0758	0.1558		0.8516	0.2146
FC_{fMRI}-$FC_{EEG-\gamma}$	0.0312	0.0794		0.88	0.0724
All subjects > 9 subjects					
FC_{fMRI}-$FC_{EEG-\delta}$	0.0682	0.192	0.0678		0.0116
FC_{fMRI}-$FC_{EEG-\theta}$	0.015	0.2226	0.0814		0.0076
FC_{fMRI}-$FC_{EEG-\alpha}$	0.0388	0.254	0.0292		0.0056
FC_{fMRI}-$FC_{EEG-\beta}$	0.0064	0.2548	0.0682		0.0098
FC_{fMRI}-$FC_{EEG-\gamma}$	**<0.0002**	0.0938	**0.0212**		**0.0006**

*SI Table 6:P-values of permutation tests comparing the crossmodal FC_{fMRI}-FC_{EEG} correlation using the complete subject session vs. the first 5 minutes and using the average connectivity over all subjects vs. the first 9 subjects (5000 iterations, Bonferroni-corrected significance level p<0.05 which corresponds to the uncorrected level p<0.05/20 = 0.0025, significant cells are marked in **bold**)*

Impact of eyes-open vs. eyes-resting state

It has been shown by Mo et al. (2013) that EEG alpha power is coupled to DMN activity when alternating between an eyes-open and an eyes-closed paradigm. We tested if we could observe any systematic changes of the crossmodal correlation between eyes-open and eyes-closed condition by permuting the labels of the different datasets (5000 permutations). As we did not measure eyes-open condition in the same subjects and setup these results should not be overinterpreted. We did not observe any significant changes of crossmodal correlation between both conditions in any frequency band (p>0.05) expect for the FC_{fMRI}-$FC_{EEG-\gamma}$ correlation (p<0.0002). Those changes in FC_{fMRI}-$FC_{EEG-\gamma}$ most likely stem from the general higher crossmodal correlation of FC_{fMRI}-$FC_{EEG-\gamma}$ for the datasets of the eyes-open condition (64Ch-1.5T and 64Ch-7T, see *Fig 2*). As such we did not observe any systematic connectivity differences especially for FC_{fMRI}-$FC_{EEG-\alpha}$, in line with our previous results when analyzing FC dynamics (Wirsich et al., 2020b). We conclude that the FC_{fMRI}-FC_{EEG} crossmodal correlation might be primarily capturing the intrinsic coupling networks (ICN) linked to canonical ICNs (Yeo et al., 2011), which are preserved across eyes-open vs. eyes closed resting state.